Electronic Supplementary Information

Multi-Stimuli Programmable FRET† based RGB Absorbing Antennae Towards Ratiometric Temperature, pH and Multiple Metal Ion Sensing

Kavita Rani and Sanchita Sengupta*[a]

[a] Department of Chemical Sciences

Indian Institute of Science Education and Research (IISER) Mohali

Knowledge City, Sector 81, Manauli, Punjab (140306), India

E-mail: sanchita@iisermohali.ac.in

Table of Contents

1. Experimental Procedures

1.1 Materials and Methods

All chemicals and solvents were purchased from commercial suppliers and used without further purification. Dichloromethane (DCM) was dried over calcium hydride and distilled prior to use. Tetrahydrofuran (THF) was dried over sodium/benzophenone and distilled prior to use. Silica gel of mesh size 60-120 was used for column chromatography. The ^{1}H and ^{13}C NMR spectra were recorded on Bruker Biospin Avance III FT-NMR 400 MHz spectrometer at room temperature. Tetramethyl silane was used as internal standard.

The high-resolution mass spectra were recorded with Waters QTOF mass spectrometer. Software used for acquiring mass spectra was Flex Control, Bruker (USA) and software used for analysing mass spectra was Flex Analysis 3.1.

UV-Vis and near-infrared (NIR) spectral measurements were carried out with Carey 5000 UV/Vis spectrophotometer using a quartz cuvette with 1 cm path length. The steady state emission and excitation studies were performed with Hitachi F7000 fluorescence spectrophotometer equipped with R928F photomultiplier expandable up to 900 nm.

Temperature dependent fluorescence of samples were measured using temperature-controlled cuvette holder for Hitachi F7000 spectrophotometer (Luma 40) from Quantum Northwest. The Luma 40 was used in the temperature range of -20 ºC to 60ºC.

Temperature dependent absorption spectra of samples were measured using Agilent Cary 60 UV/Vis spectrophotometer equipped with single cell Peltier accessory.

The electrochemical measurements were recorded using CHI-610 electrochemical workstation from CH Instruments (USA), with a conventional three electrode single-compartment cell consisting of a glassy carbon as the working electrode, Ag/AgCl containing 1M KCl solution as the reference electrode, Pt wire as the counter electrode and ferrocene was used for internal calibration. Cyclic voltammetry measurements were performed at a scan-rate of 100 mV/s. Tetrabutylammonium hexafluorophosphate (TBAHFP) (Alfa Aesar) (0.1 M) dissolved in pre-dried DCM was used as supporting electrolyte. The solutions were purged with nitrogen prior to all measurements. The electrochemical potential was internally calibrated against the standard ferrocene/ferrocenium (Fc/Fc^{+}) redox couple prior to each measurement.

Time resolved fluorescence spectra were measured by time correlated single photon counting (TCSPC) model from Fluorocube, Horiba Jobin Yvon, NJ equipped with picosecond laser diodes as excitation source. The 440 nm and 560 nm lasers were used as a light source for the excitation of samples and the instrument response function (IRF) was collected using Ludox (colloidal silica) solution. The width (FWHM) of IRF was ~ 250 ps and the optical pulse durations from < 70 ps were used. Highly integrated picosecond PMT modules as well as micro channel plate PMTs were used for the time resolution.

Spectroelectrochemical measurements were performed using a cell assembly (SEC-C) supplied by BAS Inc (Japan) and the assembly comprised of a Pt counter electrode, a Pt gauze working electrode, and an Ag/AgCl reference electrode in a 1.0 mm path length quartz cell. The absorption spectra were measured using an ocean optics set up connected in absorbance mode and using FLAME spectrometer. Voltages were swept in the range of -2.0 V to +2.0 V, dry DCM was used as solvent and TBAHFP was used as the supporting electrolyte. The solutions were purged with nitrogen for 10 min prior to the Spectroelectrochemical measurements. ITO coated substrates were purchased from Xinyang technology (15 Ω/cm^2) and washed and sonicated with isopropanol and ethanol prior to use.

Fourier transform infrared (FTIR) spectra were recorded on a Perkin Elmer Spectrum Two in the range of 400 to 4000 cm^{-1} by using KBr cell.

pH was measured with LAB INDIA pH cum conductivity meter (Sr. No. PC14360507) instrument.

Buffer capsules of pH 7.00 were purchased from Sigma-Aldrich and of pH 4.00 and 9.20 were purchased from Fischer Scientific.

Poly(methyl methacrylate) (PMMA) (M_w ~120,000) was purchased from Sigma and used as received without further purification.

1.2. Synthetic procedures

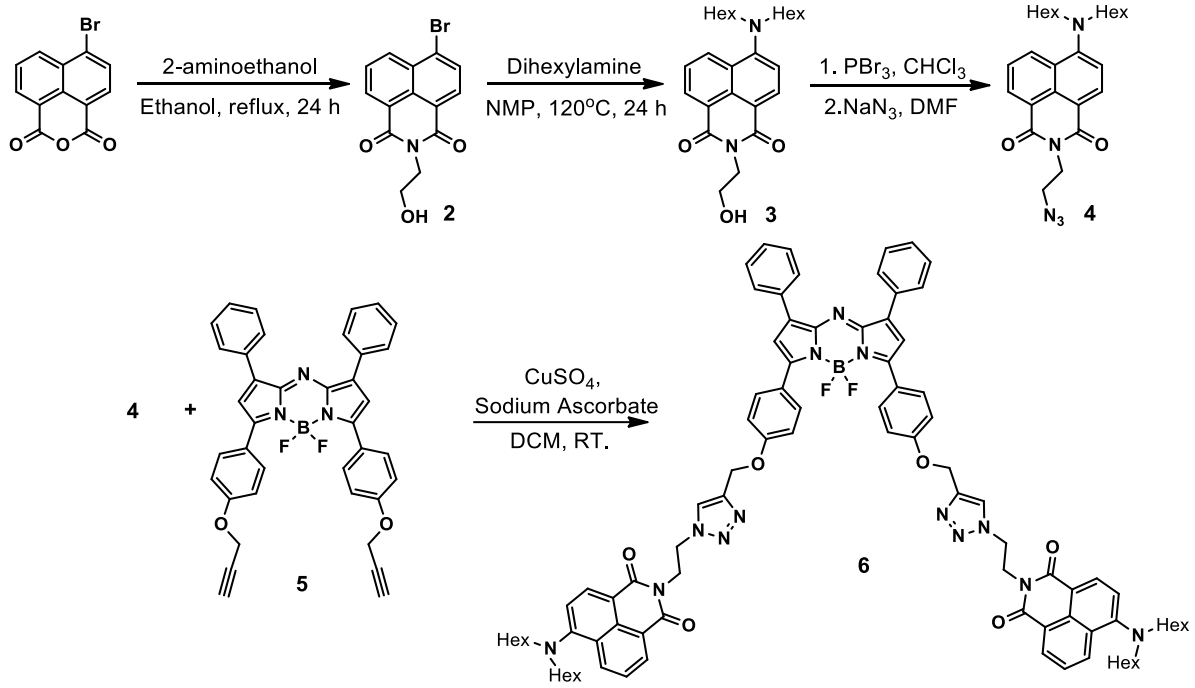

Scheme S1. Synthesis of RB compound **6**.

Synthesis of compound 2

A mixture of 4-bromo-1,8-naphthalic anhydride (1 g, 3.61 mmol) and ethanolamine (223 mg, 3.61 mmol) in ethanol (40 mL) was refluxed for 24 hours (h). After that the reaction mixture was filtered after being cooled to room temperature (RT) and the residue was washed with ethanol and dried to obtain compound **2** as an off-white solid compound with a yield of 94 %.

^{1}H NMR (400 MHz, DMSO-d$_6$): δ (ppm) = 8.56 (t, *J* = 8 Hz, 2 H), 8.34 - 8.32 (m, 1 H), 8.23 - 8.21 (m, 1 H), 8.00 (t, *J* = 8Hz, 1 H), 4.83 (t, *J* = 4 Hz, 1 H), 4.14 (t, *J* = 4 Hz, 2 H), 3.64 - 3.60 (m, 2 H).

HRMS (ESI): *m/z* calcd for $C_{14}H_{11}BrNO_3^+$ $(M+H)^+$: 319.9917; Found: 319.9922.

Synthesis of compound 3

Compound **2** (1 g, 3.12 mmol), dihexylamine (5.83 mL, 25 mmol) and N-methyl-2-pyrrolidone (NMP) (30 mL) were taken in a two-neck round-bottomed (RB) flask under nitrogen atmosphere and the reaction mixture was stirred at 120 ^{o}C for 24 h. After being cooled to room temperature, an aqueous solution of 2 M HCl was added to the reaction mixture, and precipitate was formed which was filtered and washed with water up to neutral pH and then purified by silica gel column chromatography by eluting with hexane / ethyl acetate (3 / 1 v/v) and a yellow dense liquid compound was obtained in 68 % yield.

^{1}H NMR (400 MHz, CDCl$_3$): δ (ppm) = 8.42 (d, *J* = 8 Hz, 1 H), 8.34 (dd, *J* = 20, 8 Hz, 2 H), 7.52 (t, *J* = 8 Hz, 1 H), 7.08 (d, *J* = 8 Hz, 1 H), 4.33 (t, *J* = 5 Hz, 2 H), 3.94 - 3.85 (m, 2 H), 3.28 (t, *J* = 4 H), 1.57 - 1.47 (m, 4 H), 1.23 - 1.13 (m, 12 H), 0.79 - 0.74 (m, 6 H).

^{13}C NMR (100 MHz, CDCl$_3$): δ (ppm) = 165.13, 164.66, 155.81, 132.31, 131.13, 131.03, 130.20, 126.64, 124.81, 122.63, 116.31, 114.57, 61.33, 53.53, 42.41, 31.42, 29.60, 26.69, 22.45, 13.87.

HRMS (ESI): *m/z* calcd for $C_{26}H_{37}N_2O_3^+$ $(M+H)^+$: 425.2799; Found: 425.2813.

Synthesis of compound 4

Compound **3** (900 mg, 2.12 mmol) was dissolved in dry chloroform and PBr_3 (0.30 mL, 3.18 mmol) was added dropwise at 0 ^{o}C after that reaction mixture was refluxed for ~5 h and then extracted with chloroform and the organic layer was dried over sodium sulphate and solvent was removed under reduced pressure. The intermediate compound was dissolved in dimethyl formamide (DMF), sodium azide (551 mg, 8.5 mmol) was added and reaction mixture was heated at 80 ^{o}C for overnight. After cooling down to room temperature, the reaction mixture was extracted with DCM and dried over sodium sulphate, solvent was removed under reduced pressure. The crude product was purified by column chromatography by eluting with hexane / ethyl acetate (3/1 v/v), yellow coloured dense liquid compound was obtained in 39 % yield.

^{1}H NMR (400 MHz, $CDCl_3$): δ (ppm) = 8.52 - 8.49 (m, 1 H), 8.45 - 8.37 (m, 2 H), 7.58 (t, *J* = 8 Hz, 1 H), 7.16 - 7.13 (m, 1 H), 4.36 (t, *J* = 8 Hz, 2 H), 3.59 (t, *J* = 8 Hz, 2 H), 3.31 (t, *J* = 8 Hz, 4 H), 1.58 - 1.51 (m, 4 H), 1.25 - 1.16 (m, 12 H), 0.79 - 0.76 (m, 6 H).

^{13}C NMR (100 MHz, $CDCl_3$): δ (ppm) = 164.43, 163.81, 155.88, 132.30, 131.18, 131.16, 130.32, 126.86, 124.91, 122.62, 116.45, 114.60, 53.60, 48.84, 38.48, 31.46, 26.95, 26.73, 22.49, 13.91.

HRMS (ESI): *m/z* calcd for $C_{26}H_{36}N_5O_2^+$ $(M+H)^+$: 450.2864 ; Found: 450.2884.

Synthesis of compound 5

Compound **5** was synthesized as reported in the literature.[S1,S2]

Synthesis of compound 6

The compound **4** (120 mg, 0.27 mmol) was dissolved in a mixture of DCM, ethanol (EtOH) and water (12:1:1) under nitrogen atmosphere followed by addition of sodium ascorbate (19 mg, 0.10 mmol) and copper sulphate (12 mg, 0.05 mmol) to this mixture. After purging the reaction mixture with nitrogen for 15 minutes, compound **5** (62 mg, 0.10 mmol) was added and the reaction mixture was stirred for 36 h at room temperature under nitrogen atmosphere. After completion of the reaction by monitoring with thin layer chromatography (TLC), reaction mixture was extracted with DCM, the organic layer was dried over sodium sulphate and solvent was removed under reduced pressure. The crude was purified by column chromatography DCM / Hexane (9/1 v/v) as eluent and dark green solid compound was obtained in 78 % yield.

^{1}H NMR (400 MHz, $CDCl_3$): δ (ppm) = 8.49 (d, *J* = 8 Hz, 2 H), 8.42 - 8.36 (m, 4 H), 8.07 (t, *J* = 8 Hz, 8 H), 7.81 (s, 1 H), 7.61 (t, *J* = 8 Hz, 2 H), 7.48 - 7.40 (m, 6 H), 7.14 (d, *J* = 8 Hz, 2 H), 7.07 (t, J = 8 Hz, 6 H), 5.28 (s, 4 H), 4.78 (t, *J* = 8 Hz, 4 H), 4.68 (t, *J* = 8 Hz, 4 H), 3.33 (t, *J* = 8 Hz, 8 H), 1.58 - 1.53 (m, 8 H), 1.27 - 1.20 (m, 24 H), 0.83 (t, J = 4 Hz, 12 H).

^{13}C NMR (100 MHz, $CDCl_3$): δ (ppm) = 164.54, 163.87, 160.76, 158.16, 156.24, 145.44, 143.88, 143.21, 132.66, 132.57, 131.79, 131.54, 130.59, 129.38, 129.34, 128.67, 127.04, 125.13, 124.55, 123.59, 122.54, 118.79, 116.64, 115.20, 114.42, 62.24, 53.80, 48.25, 39.53, 31.65, 27.12, 26.91, 22.69, 14.11.

HRMS (ESI): *m/z* calcd for $C_{90}H_{97}BF_2N_{13}O_6^+$ $(M+H)^+$: 1504.7740 ; Found: 1504.7700.

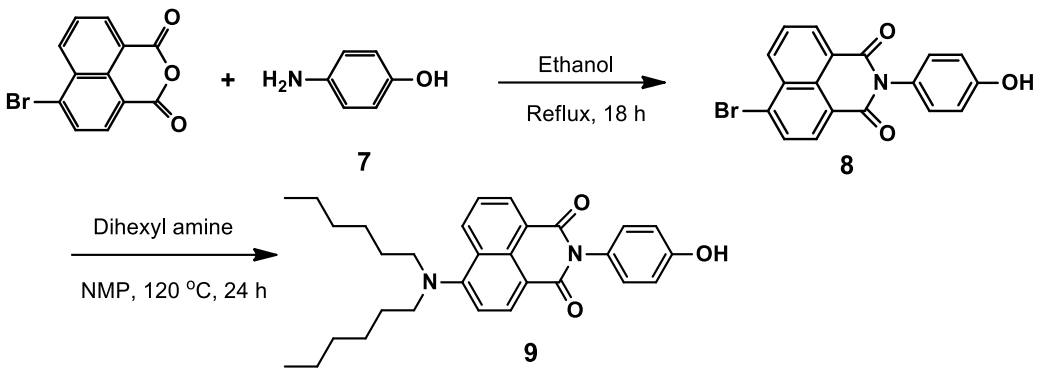

Scheme S2. Synthesis of compound **9**.

Synthesis of compound 8

A mixture of 4-bromo-1,8-naphthalic anhydride (3 g, 10.83 mmol) and 4-aminophenol (1.41 g, 12.90 mmol) in EtOH (80 mL) was refluxed for around 24 h. The reaction mixture was filtered after being cooled to room temperature. Subsequently, the residue was washed with ethanol and dried in vacuum oven to obtain compound **8** as an off-white solid compound with a yield of 92 %.[S3]

^{1}H NMR (400 MHz, DMSO-d_6): δ (ppm) = 9.69 (s, 1 H), 8.57 (t, *J* = 8 Hz, 2 H), 8.33 (d, *J* = 8 Hz, 1 H), 8.24 (d, *J* = 8 Hz, 1 H), 8.02 (t, *J* = 8 Hz, 1 H), 7.14 (d, *J* = 8 Hz, 2 H), 6.87 (d, *J* = 8 Hz, 2 H).

Synthesis of compound 9

Compound **8** (3 g, 8.15 mmol), dihexylamine (9.06 g, 48.88 mmol) and N-methyl-2-pyrrolidone (NMP) (30 mL) were taken in a two-neck round-bottomed (RB) flask under nitrogen atmosphere and the reaction mixture was stirred at 120 °C for 24 h. After being cooled to room temperature, an aqueous solution of 2 M HCl was added to the reaction mixture, and a gel-like mixture was formed which was filtered and then purified by silica gel column chromatography by eluting with hexane / ethyl acetate (3 / 1 v/v) and compound **9** was obtained as a yellow solid in 60 % yield.

^{1}H NMR (400 MHz, $CDCl_3$): δ (ppm) = 8.63 (d, *J* = 8 Hz, 1 H), 8.53 (d, *J* = 8 Hz, 1 H), 8.48 (d, *J* = 8 Hz, 1 H), 7.69 (t, *J* = 8 Hz, 1 H), 7.22 (d, *J* = 8 Hz, 1 H), 7.08 (d, *J* = 12 Hz, 2 H), 6.83 (d, *J* = 8 Hz, 2 H), 6.27 (s, 1 H), 3.39 (t, *J* = 8 Hz, 4 H), 1.65 - 1.58 (m, 4 H), 1.31 - 1.26 (m, 12 H).

^{13}C NMR (100 MHz, $CDCl_3$): δ (ppm) = 165.57, 165.10, 156.63, 156.36, 133.00, 131.89, 131.63, 130.88, 129.37, 127.35, 127.11, 125.23, 123.24, 116.94, 116.75, 115.04, 53.87, 31.66, 27.17, 26.94, 22.69, 14.12.

HRMS (ESI): *m/z* calcd for $C_{30}H_{37}N_2O_3^+$ $(M+H)^+$: 473.2799 ; Found: 473.2813.

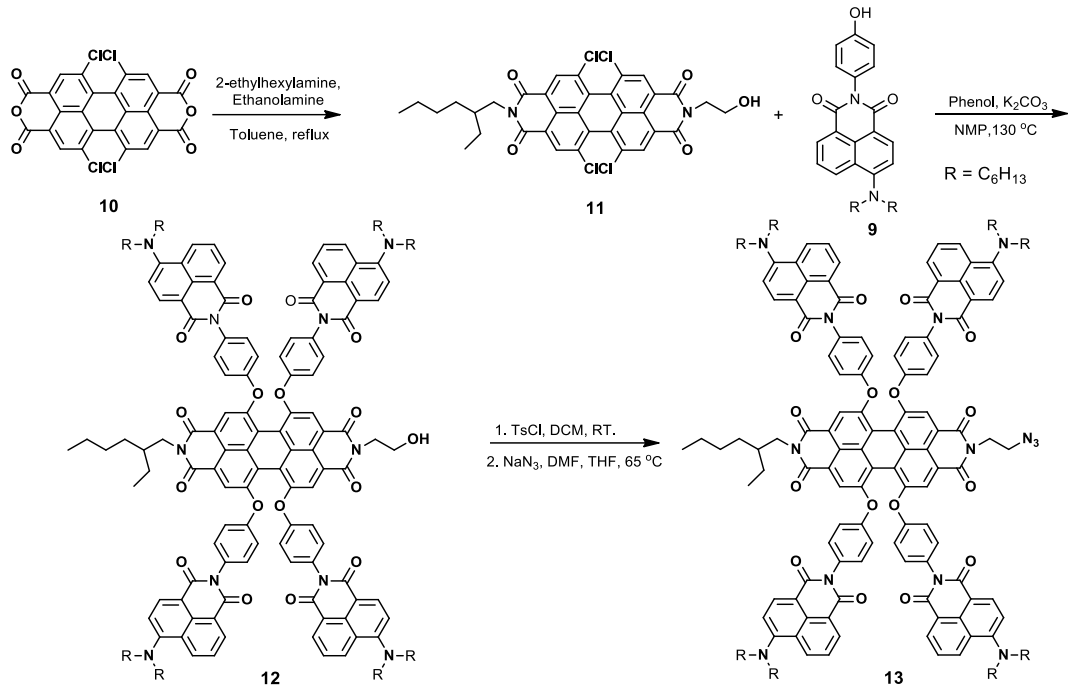

Scheme S3. Synthesis of energy donor GB compound **13**.

Synthesis of compound 10 and 11

Compounds **10** and **11** were synthesized according to published procedure. [S1]

Synthesis of compound 12

Compounds **11** (300 mg, 0.44 mmol), **9** (1657 mg, 3.51 mmol) and K_2CO_3 (727 mg, 5.26 mmol) were dissolved in dry N-methyl-2-pyrrolidone (NMP) under nitrogen atmosphere in a two-neck round bottom flask. The reaction mixture was stirred for 48 h at 130 °C. After being cooled to room temperature, 2 M HCl was added and precipitate was formed that was filtered and washed with water/methanol mixture. Subsequently, crude product was purified by column chromatography with chloroform / ethyl acetate (EA) (9/1) as eluent to obtain **12** as a purple solid in 33 % yield.[S4]

^{1}H NMR (400 MHz, $CDCl_3$): δ (ppm) = 8.55 - 8.51 (m, 8 H), 8.48 - 8.43 (m, 8 H), 7.62 (t, *J* = 8 Hz, 4 H), 7.29 - 7.27 (m, 8 H), 7.19 (d, *J* = 8 Hz, 4 H), 7.08 - 7.04 (m, 8 H), 4.50 (t, *J* = 8 Hz, 2 H), 4.20 - 4.08 (m, 2 H), 4.02 - 3.98 (m, 2 H), 3.35 (t, *J* = 8 Hz , 16 H), 1.98 - 1.95 (m, 1 H), 1.62 - 1.55 (m, 20 H), 1.41 - 1.26 (m, 52 H), 0.96 - 0.88 (m, 6 H), 0.87 - 0.82 (m, 24 H).

^{13}C NMR (100 MHz, $CDCl_3$): δ (ppm) = 164.73, 164.19, 164.02, 163.45, 156.08, 155.95, 155.88, 155.87, 154.99, 154.66, 132.67, 132.64, 132.53, 131.52, 131.48, 131.21, 130.80, 130.72, 127.32, 125.18, 123.81, 123.46, 123.13, 122.87, 122.50, 121.93, 121.15, 120.84, 120.74, 119.27, 116.85, 115.61, 115.58, 62.01, 53.86, 38.03, 31.68, 30.90, 28.84, 27.14, 26.95, 24.17, 23.23, 22.70, 14.32, 14.12, 10.79.

MS (MALDI-TOF): *m/z* calcd for $C_{154}H_{167}N_{10}O_{17}^{+}$ $(M+H)^{+}$: 2428.2505 ; Found: 2428.4614.

Synthesis of compound 13

Compound **12** (225 mg, 0.09 mmol) was dissolved in dry DCM (20 mL), 4-dimethyl amino pyridine (1 mg, 0.01 mmol) was added to this solution. After cooling this mixture to 0 ^{o}C, p-toluene sulfonyl chloride (70 mg, 0.37 mmol) and triethyl amine (0.08 mL, 0.56 mmol) were added under nitrogen atmosphere. The mixture was stirred for 24 h at room temperature under nitrogen atmosphere. After the completion of the reaction, the reaction mixture was diluted with DCM, washed with aqueous sodium bicarbonate and saturated sodium chloride solutions. The organic layer was dried over sodium sulphate and solvent was removed under reduced pressure. The crude product was dissolved in dry tetrahydrofuran (THF) (20 mL) followed by addition of sodium azide (24 mg, 0.37 mmol) after dissolving in dry dimethyl formamide (DMF) under nitrogen atmosphere, the reaction mixture was stirred at 65 ^{o}C overnight. After being cooled to room temperature, reaction mixture was extracted with DCM and dried over sodium sulphate, purified by column chromatography with DCM / EA (9/1 v/v) as eluent and a purple solid compound was obtained in 29 % yield.

^{1}H NMR (400 MHz, $CDCl_3$): δ (ppm) = 8.55 - 8.52 (m, 8 H), 8.48 - 8.44 (m, 8 H), 7.62 (t, *J* = 8 Hz, 4 H), 7.30 - 7.28 (m, 8 H), 7.19 (d, *J* = 8 Hz, 4 H), 7.07 - 7.04 (m, 8 H), 4.46 (t, *J* = 8 Hz, 2 H), 4.17 - 4.04 (m, 2 H), 3.68 (t, *J* = 8 Hz , 2 H), 3.35 (t, *J* = 8 Hz, 16 H), 1.99 - 1.93 (m, 1 H), 1.62 - 1.55 (m, 20 H), 1.41 - 1.24 (m, 52 H), 0.96 - 0.88 (m, 6 H), 0.87 - 0.82 (m, 24 H).

^{13}C NMR (100 MHz, $CDCl_3$): δ (ppm) = 164.71, 164.17, 163.42, 163.10, 156.07, 155.97, 155.85, 154.95, 154.66, 132.75, 132.68, 132.51, 131.48, 131.19, 130.80, 130.73, 127.33, 125.18, 123.82, 123.48, 123.06, 122.86, 122.51, 121.94, 121.20, 120.89, 120.76, 119.24, 116.86, 115.61, 53.87, 48.87, 38.04, 31.68, 30.91, 28.84, 27.14, 26.96, 24.17, 23.23, 22.70, 14.32, 14.12, 10.79.

MS (MALDI-TOF): *m/z* calcd for $C_{154}H_{166}N_{13}O_{16}^{+}$ $(M+H)^{+}$: 2453.2570 ; Found: 2453.5115.

Synthesis of RGB antenna 1

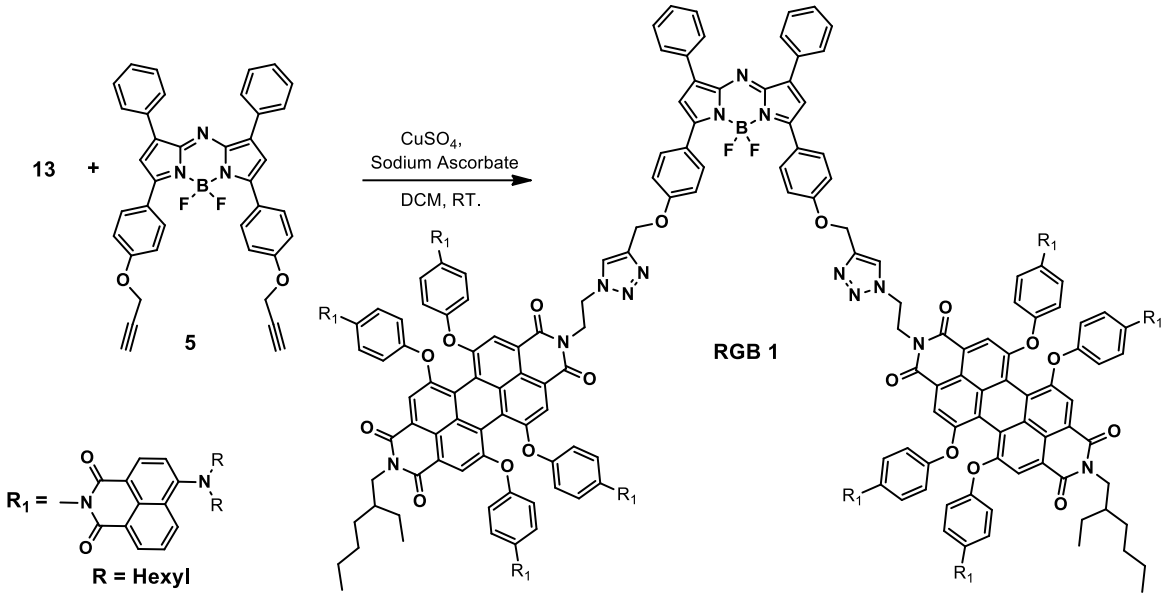

Scheme S4. Synthesis of RGB antenna **1**.

The compound **13** (65 mg, 0.03 mmol) was dissolved in a mixture of DCM, EtOH and water (12:1:1) under nitrogen atmosphere followed by addition of sodium ascorbate (2 mg, 0.01 mmol) and copper sulphate (1 mg, 0.005 mmol) to this mixture. After purging the reaction mixture with nitrogen for 15 minutes, compound **5** (5 mg, 0.01 mmol) was added and the reaction mixture was stirred for 36 h at room temperature. After completion of the reaction, the reaction mixture was extracted with DCM, the organic layer was dried over sodium sulphate and solvent was removed under reduced pressure. The crude was purified by column chromatography DCM / EA (1/1 v/v) as eluent and a brown solid compound was obtained in ~ 82 % yield.

^{1}H NMR (400 MHz, $CDCl_3$): δ (ppm) = 8.53 - 8.50 (m, 12 H), 8.46 - 8.40 (m, 20 H), 8.01 (t, *J* = 8 Hz, 8 H), 7.85 (s, 2 H), 7.62 - 7.56 (m, 8 H), 7.39 - 7.33 (m, 8 H), 7.30 - 7.28 (m, 14 H), 7.15 (t, *J* = 8 Hz, 8 H), 7.10 - 7.03 (m, 20 H), 6.99 (s, 2 H), 5.30 (s, 4 H), 4.81 - 4.67 (m, 8 H), 4.17- 4.07 (m, 4 H), 3.35 - 3.30 (m, 32 H), 1.98 - 1.94 (m, 2 H), 1.61 - 1.56 (m, 40 H), 1.40 - 1.21 (m, 104 H), 0.96 - 0.88 (m, 12 H), 0.83 - 0.80 (m, 48 H).

^{13}C NMR (100 MHz, $CDCl_3$): δ (ppm) = 164.71, 164.69, 164.17, 164.16, 163.42, 162.92, 160.89, 158.20, 156.05, 155.91, 155.87, 155.83, 155.03, 154.66, 145.30, 143.93, 132.76, 132.67, 132.63, 132.54, 132.49, 132.45, 131.82, 131.79, 131.51, 131.49, 131.17, 131.16, 130.78, 130.75, 129.32, 128.54, 127.31, 127.27, 125.16, 124.45, 123.83, 123.72, 123.48, 123.44, 122.75, 122.38, 122.07, 121.10, 120.86, 120.69, 119.32, 119.29, 116.84, 116.77, 115.63, 115.53, 115.29, 62.30, 58.83, 48.14, 38.04, 31.67, 30.90, 28.84, 27.14, 26.95, 24.17, 23.23, 22.70, 14.32, 14.12, 10.79.

MS (MALDI-TOF): *m/z* calcd for $C_{346}H_{357}BF_2N_{29}O_{34}^{+}$ $(M+H)^{+}$: 5510.7153; Found: 5510.9551.

1.3 NMR spectra

^{1}H NMR spectra of Compound 2 in DMSO-d6

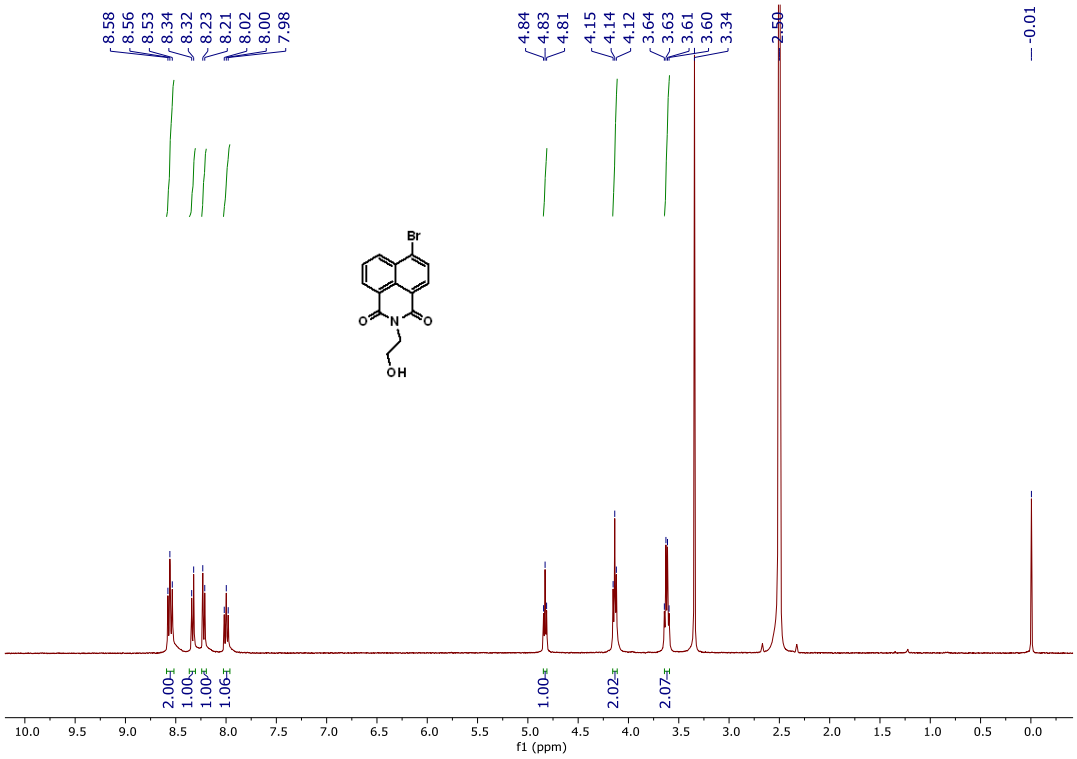

^{1}H NMR spectra of Compound 3 in $CDCl_3$

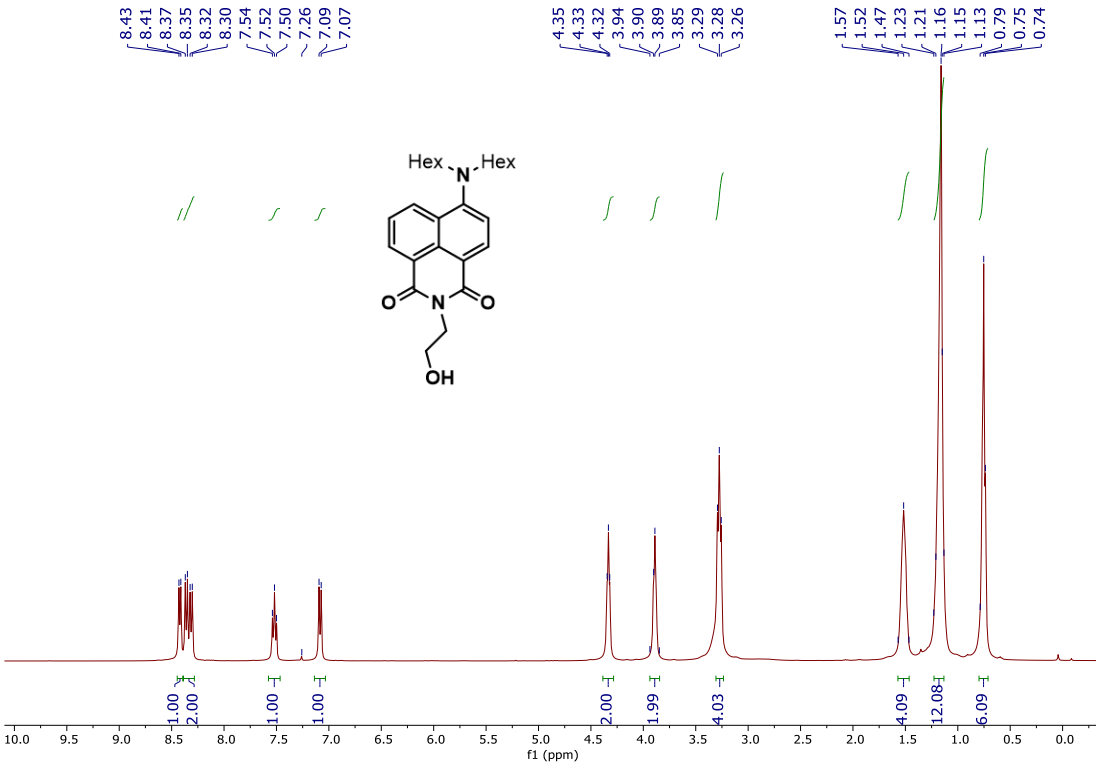

^{13}C NMR spectra of Compound 3 in $CDCl_3$

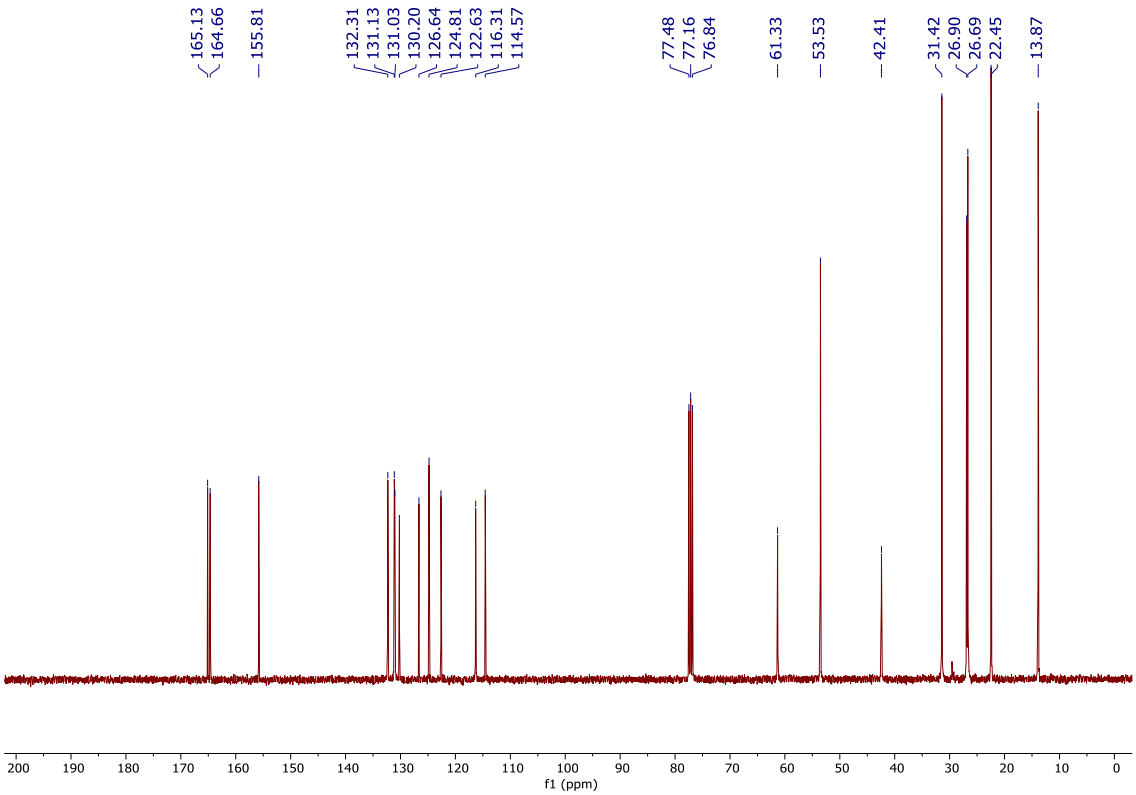

^{1}H NMR spectra of Compound 4 in $CDCl_3$

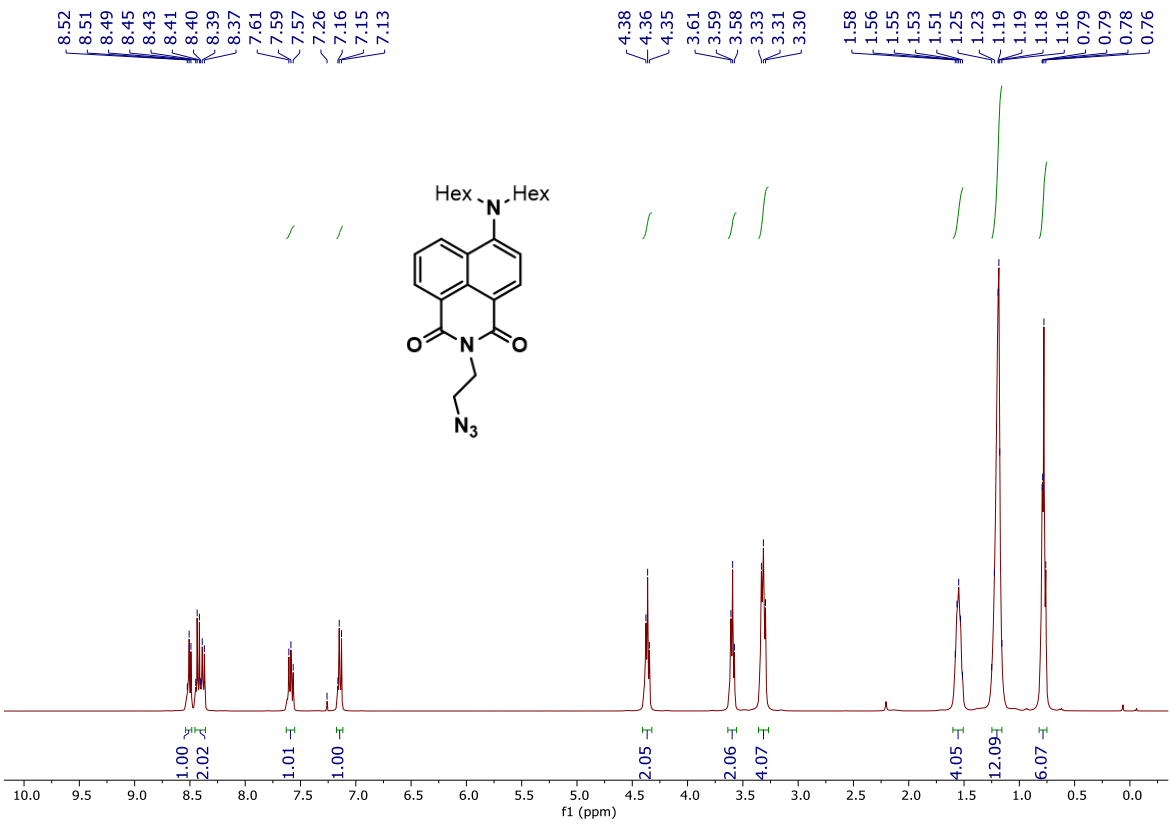

^{13}C NMR spectra of compound 4 in $CDCl_3$

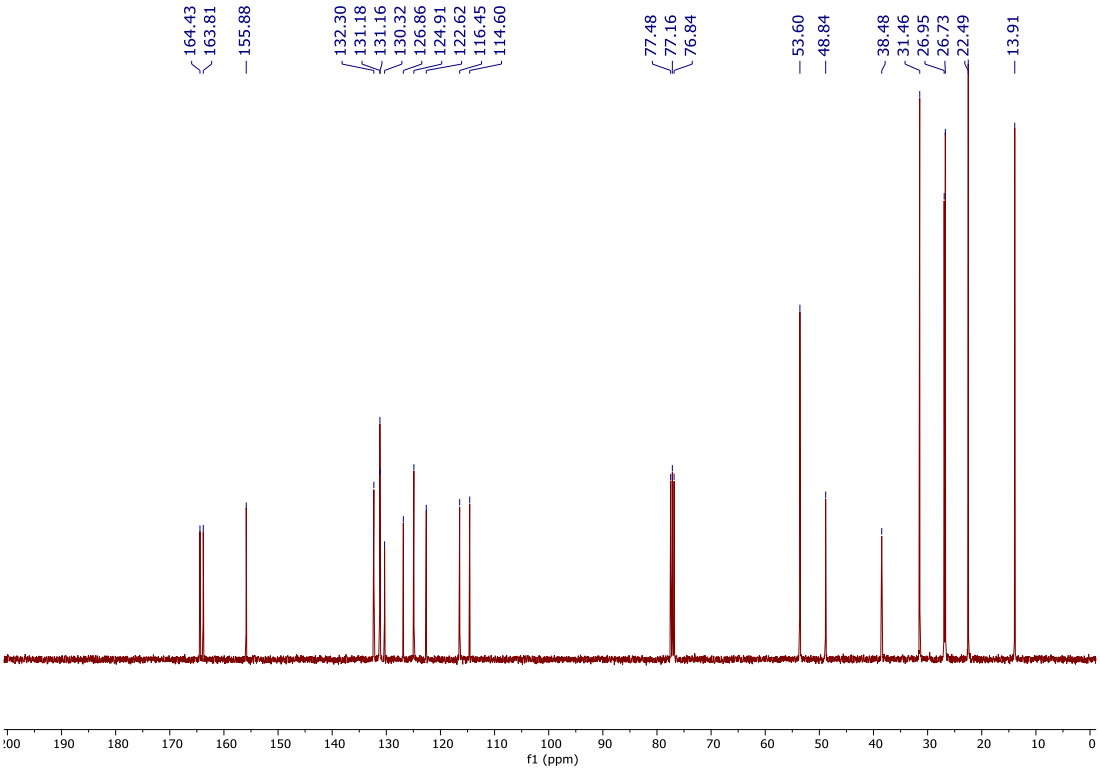

^{1}H NMR spectra of RB Compound 6 in $CDCl_3$

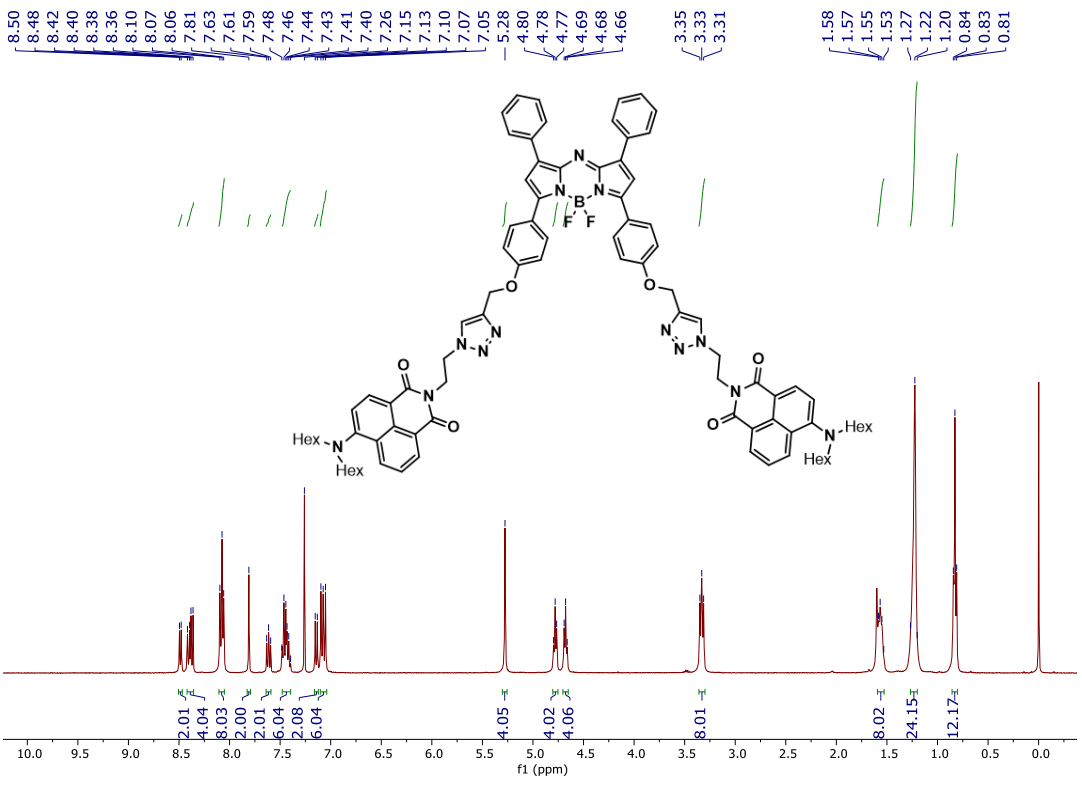

^{13}C NMR spectra of RB Compound 6 in $CDCl_3$

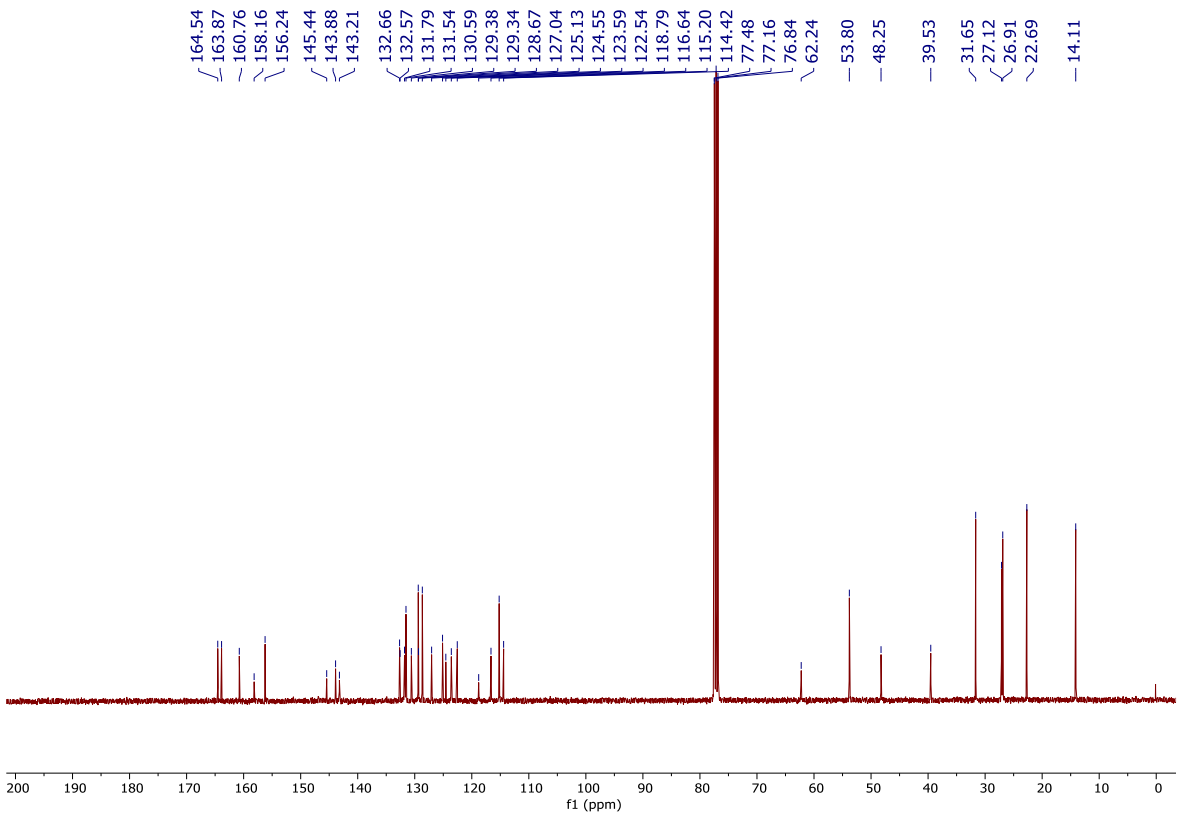

^{1}H NMR spectra of Compound 8 in DMSO-d6

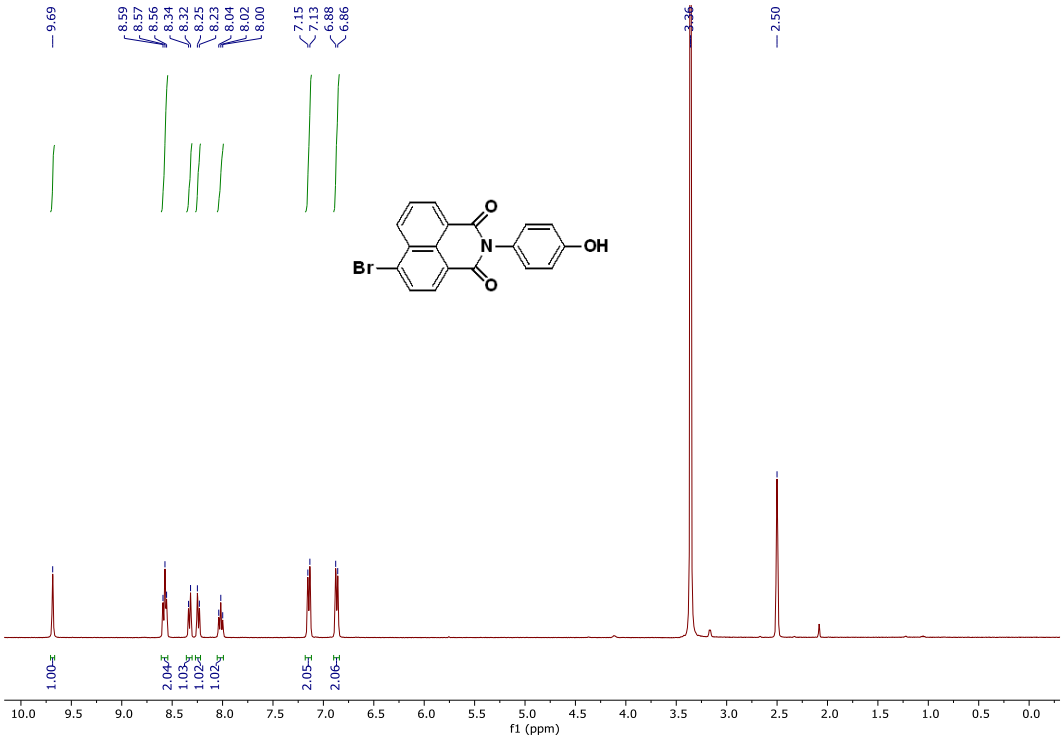

^{1}H NMR spectra of Compound 9 in $CDCl_3$

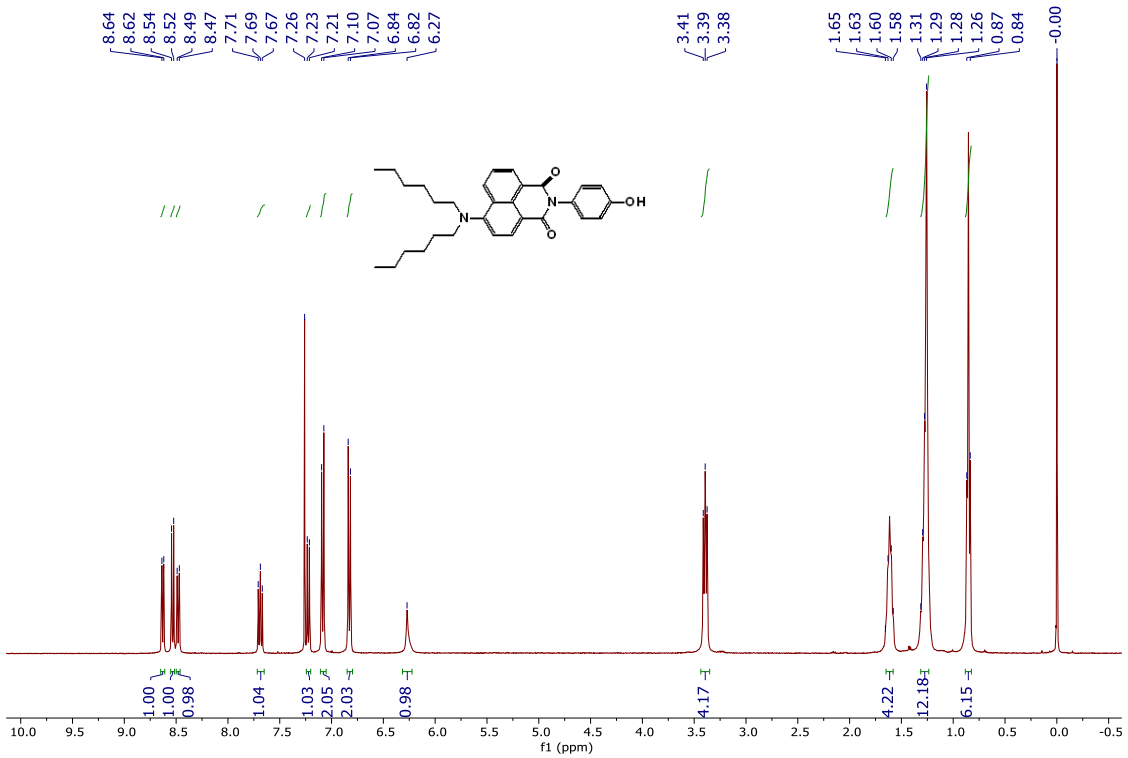

^{13}C NMR spectra of Compound 9 in $CDCl_3$

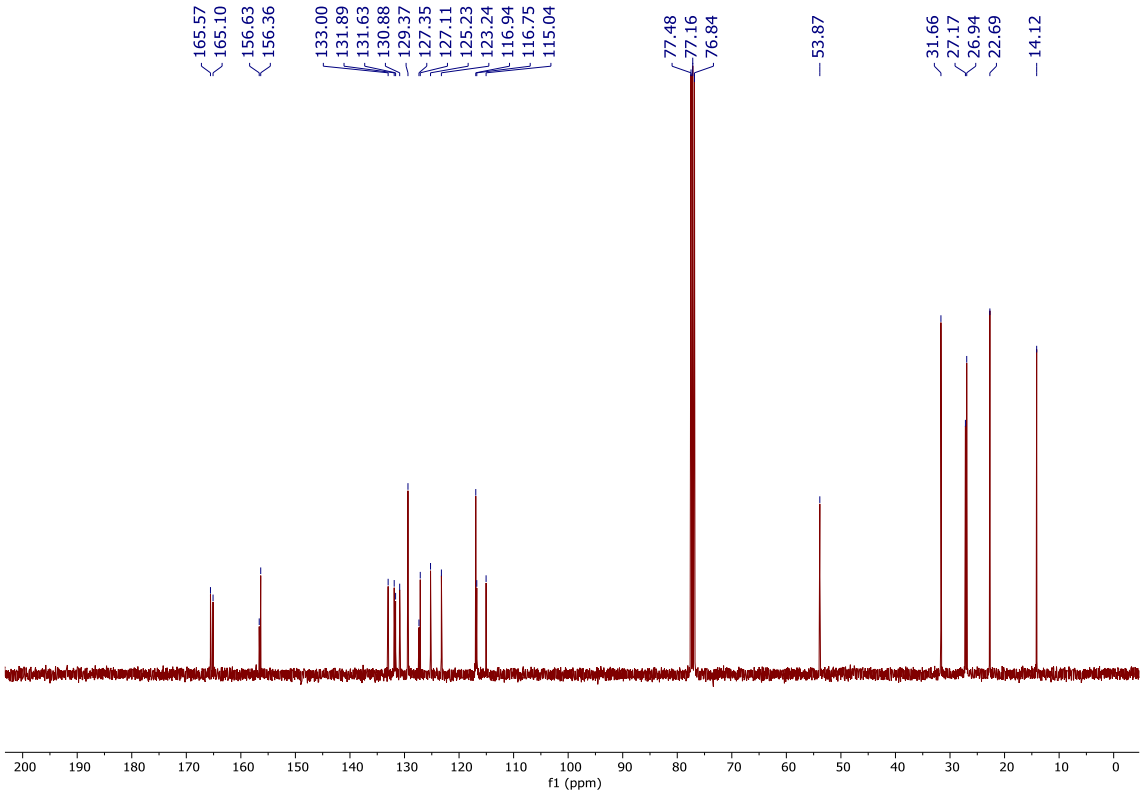

^{1}H NMR spectra of GB antenna 12 in $CDCl_3$

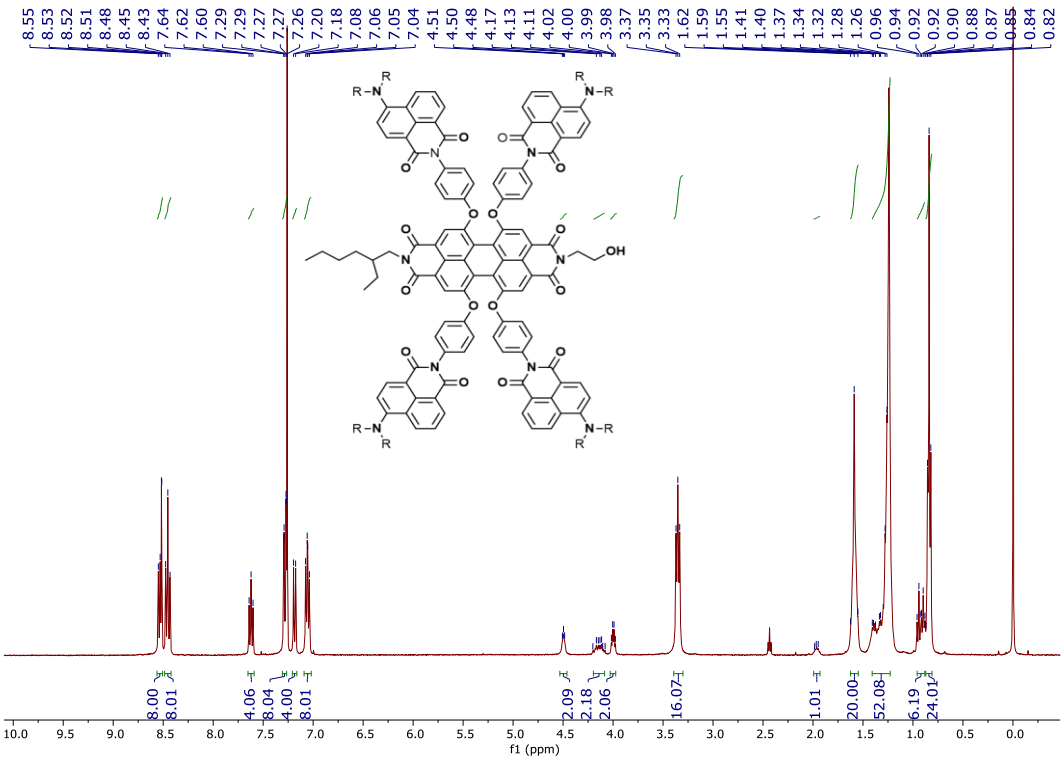

^{13}C NMR spectra of GB antenna 12 in $CDCl_3$

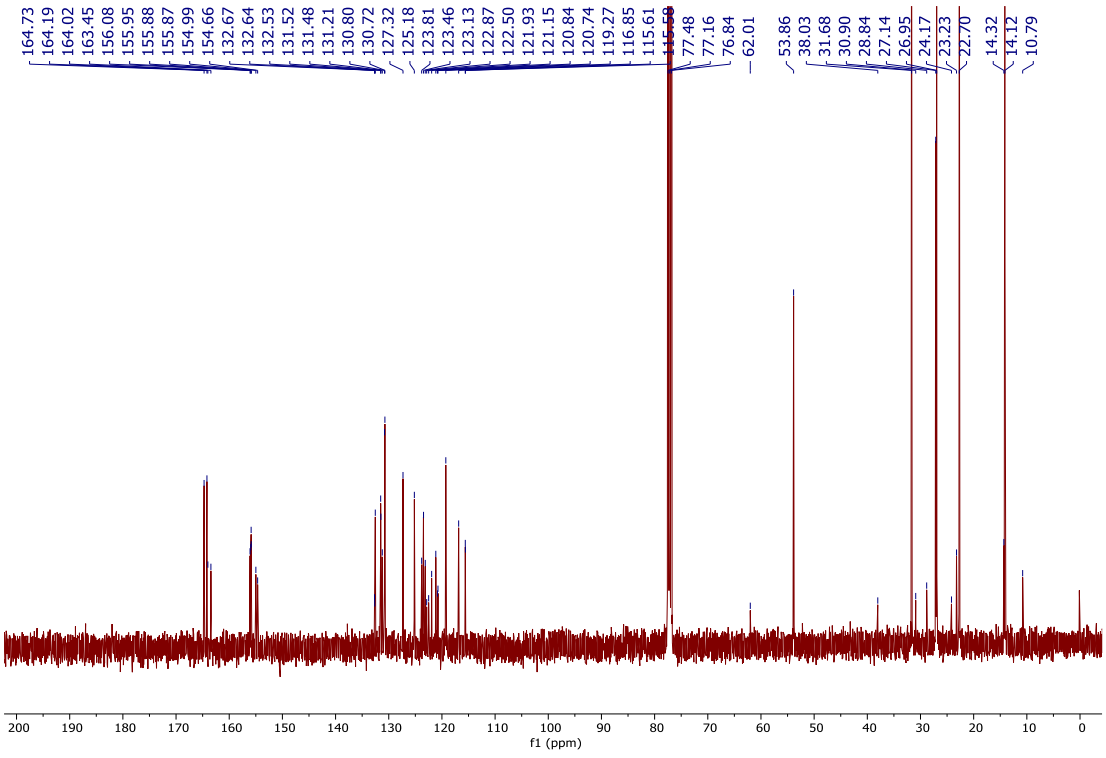

^{1}H NMR spectra of GB antenna 13 in $CDCl_3$

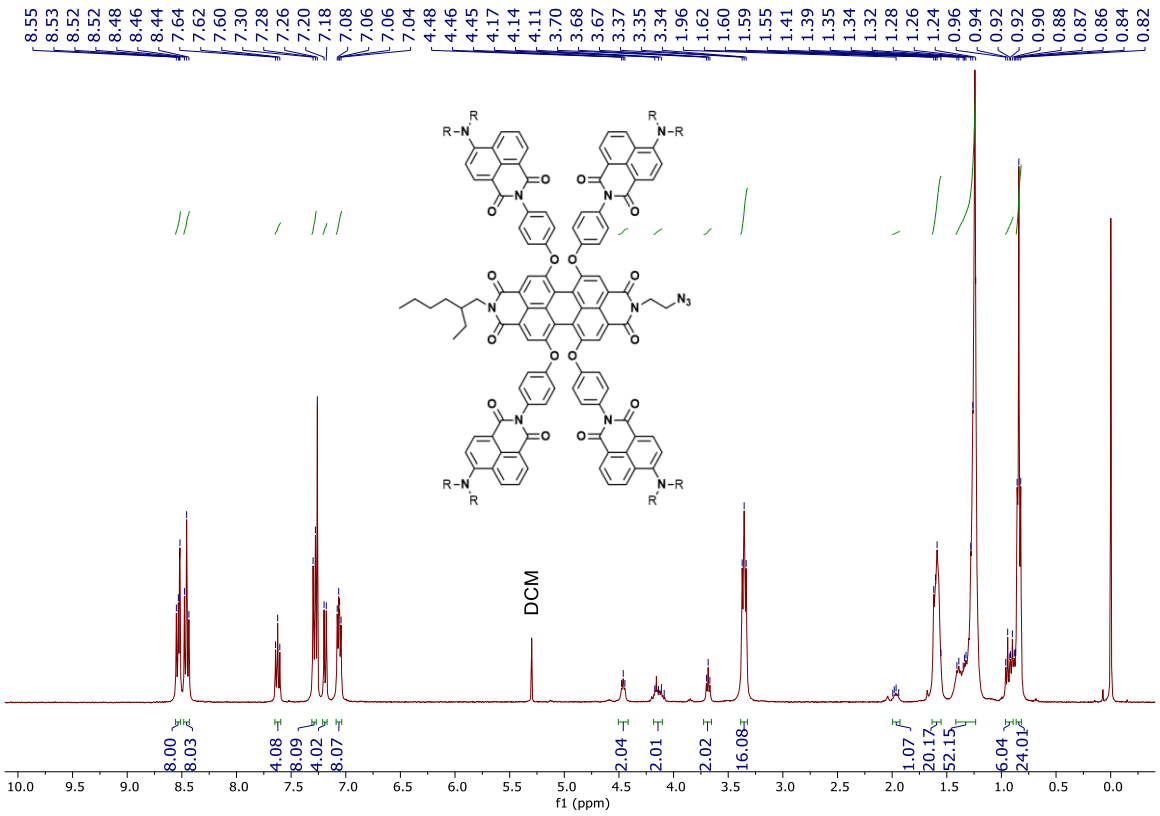

^{13}C NMR spectra of GB antenna 13 in $CDCl_3$

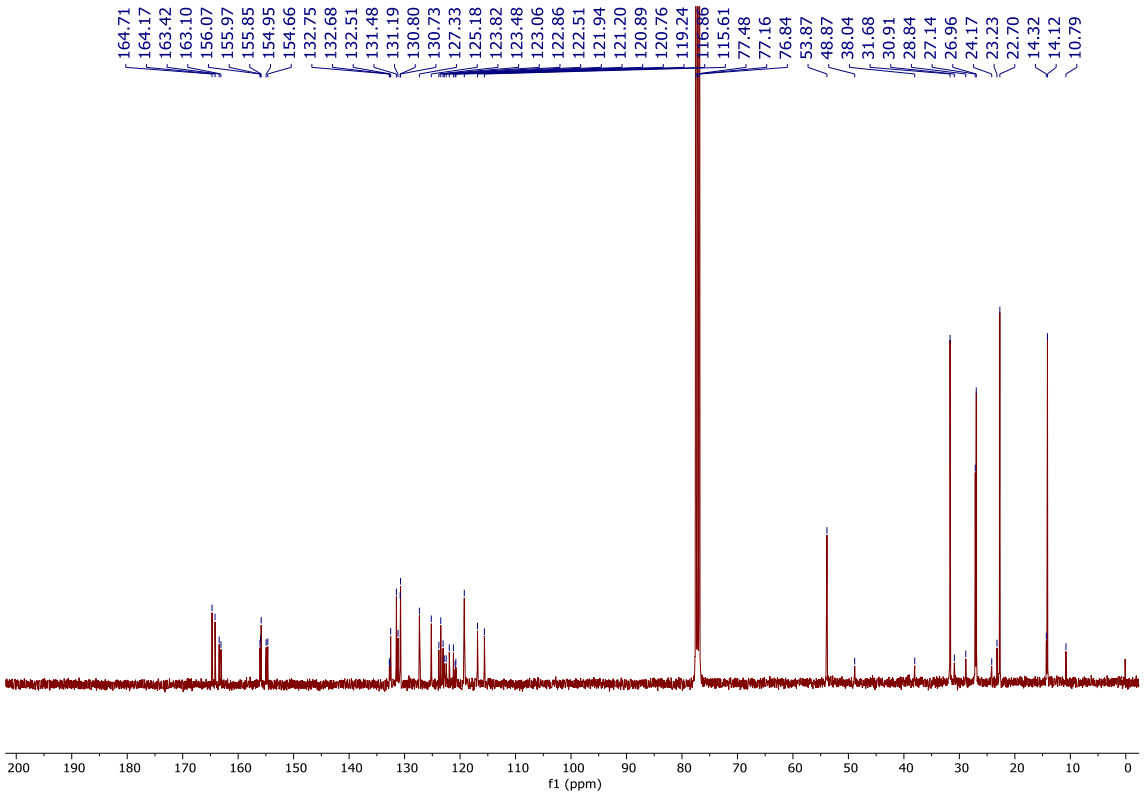

^{1}H NMR spectra of RGB antenna 1 in $CDCl_3$

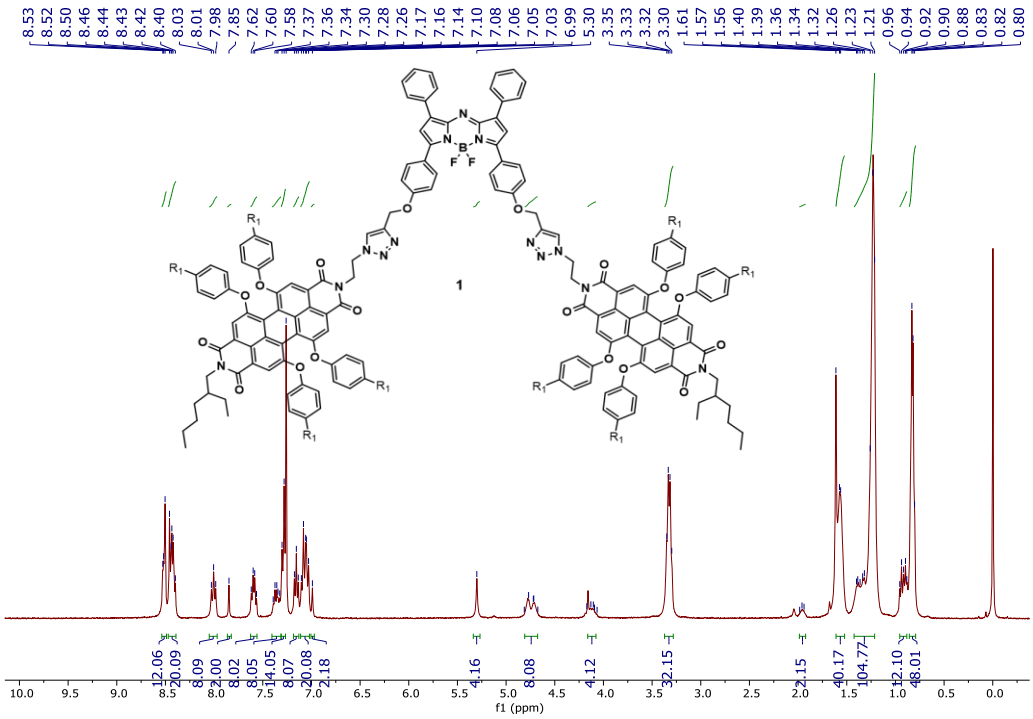

^{13}C NMR spectra of RGB antenna 1 in $CDCl_3$

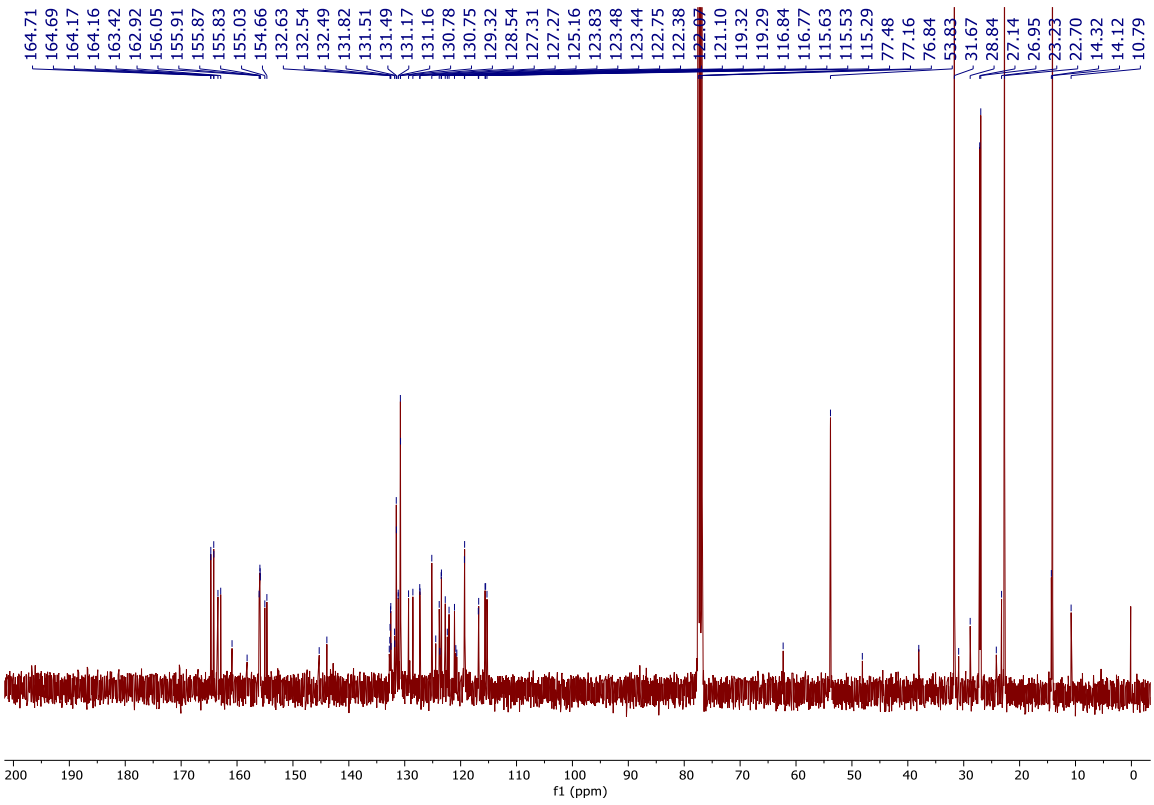

2. Photophysical characterization

2.1 Fluorescence excitation spectra

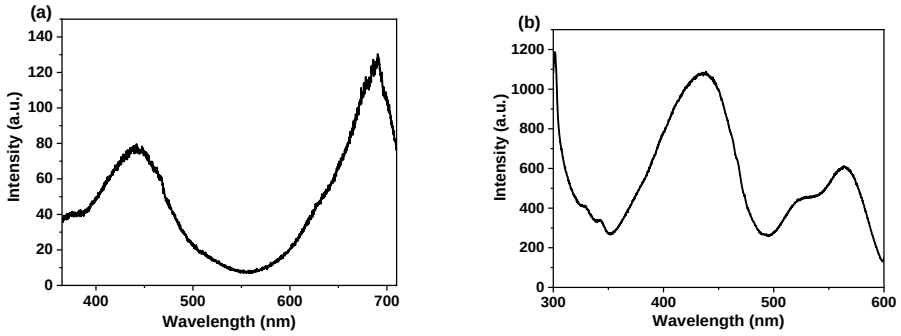

Figure S1. Fluorescence excitation spectra of (a) **RB** compound **6** and (b) **GB** compound **12** in $CHCl_3$.

The fluorescence excitation spectra for RB **6** (Figure S1a) and GB **12** (Figure S1b) were recorded by keeping emission monochromator at energy acceptor emission and the spectra contain all the peaks that of absorption spectra which clearly indicates quantitative energy transfer process from energy donor moiety Naphthalimide (Np) to energy acceptor moiety aza-BODIPY and PDI for antennae RB **6** and GB **12** respectively.

2.2 Fluorescence quantum yield

Table S1. Relative quantum yields of **9**, **6**, **12** and **1** by using relative method in $CHCl_3$.

Compound	**λ_{ex} (nm)**	**λ_{em} (nm)**	**Absorbance**			**Integrated fluorescence intensity**			**Quantum Yield** $\Phi = \Phi_R(I / I_R)(A_R / A)(\lambda_{ex.R} / \lambda_{ex})(n^2 / n_R^2)$	
			1	**2**	**3**	**1**	**2**	**3**	**Φ_i**	**Φ_{avg}**
9	430	518	0.0203	0.0338	0.0394	130.954	212.572	262.006	0.97 0.95 0.97	0.96
6	442	518	0.0080	0.0301	0.0282	0.437	1.624	1.478	0.008 0.008 0.007	0.008
	436	518	0.0306	0.0247	0.0305	2.087	1.722	1.815	0.01 0.01	0.009

12									0.008	
	564	606	0.0245	0.0132	0.0163	88.859	44.302	55.714	0.83 0.81 0.85	0.83
1	436	518	0.0732	0.0415	0.0322	0.958	1.947	0.687	0.002 0.007 0.003	0.004
	436	606	0.0388	0.0217	0.0173	17.230	9.652	9.504	0.13 0.14 0.18	0.15
	566	606	0.0388	0.0217	0.0173	12.491	7.240	7.079	0.073 0.080 0.102	0.085
Rhodamine 6G (ethanol)			0.0295	0.0474	0.0617	276.90	443.77	602.31		0.95 (reported)[S5]
Lumogen® F Red 305 (in $CHCl_3$)			0.0315	0.0394	0.0454	135.19	160.11	178.19		0.96 (reported)[S6]

Table S2. Calculation of energy transfer efficiency (ETE) from fluorescence quantum yield.

Compound	**λ_{ex}(nm)**	**λ_{em}(nm)**	**φ**	**ETE = 1- φ_{DA}/φ_{D}**
9	430	518	0.96	-
6	442	518	0.008	~ 99 %
12	436	518	0.009	~ 99 %
	436	606	1.00	
	564	606	0.83	

1	436	518	0.004	~ 99 %
	436	606	0.15	
	566	606	0.08	~ 90 %

For RB antenna **6**, energy transfer efficiency (ETE) from naphthalimide (Np) to aza-BODIPY was calculated to be ~ 99 % in $CHCl_3$ by taking Np compound **9** as the reference energy donor. Similarly for GB antenna **12**, ETE was calculated to be ~ 99 % by taking Np compound **9** as reference energy donor.

For RGB antenna **1**, ETE was calculated to be ~ 99 % from Np to PDI or aza-BODIPY or by cascade fashion from Np to PDI to aza-BODIPY by taking **9** as reference energy donor and ETE was calculated to be ~ 90 % from PDI to aza-BODIPY by taking GB **12** (λ_{ex} = 564 nm) as reference energy donor.

2.3 Fluorescence lifetime

Table S3. Fluorescence lifetime analysis of **9**, **6**, **12** and **1** at different excitation and emission wavelengths in $CHCl_3$.

Comp.	**λ_{exc}(nm)**	**λ_{em}(nm)**	**$\tau_1(\alpha_1)$(ns)**	**$\tau_2(\alpha_2)$(ns)**	**$\tau_3(\alpha_3)$(ns)**	**$\tau_4(\alpha_4)$(ns)**	**τ_{avg}(ns)**	**χ^2**
9	440	518	7.93(1.00)	-	-		7.93	1.25
5	635	712	2.96 (1.00)	-	-	-	2.96	1.02
6	440	518	1.29(0.00)	7.18(0.01)	0.027(0.99)	-	0.094	1.23
6	440	717	3.08 (1.00)	-	-	-	3.08	1.14
6	635	717	2.83 (1.00)	-	-	-	2.83	1.06
12	440	518	1.61(0.00)	7.05(0.00)	0.006(1.00)		0.006	1.05
12	440	606	0.61(0.14)	5.69(0.86)	-	-	4.97	1.19
12	560	606	5.95(1.00)	-	-	-	5.95	1.13
1	440	518	0.20(0.00)	3.05(0.00)	7.62(0.00)	0.008(1.00)	0.008	1.62
1	440	606	2.37(0.00)	5.29(0.74)	1.15(0.25)	-	4.23	1.16
1	440	721	0.78(0.19)	2.62(0.81)	-	-	2.27	1.14
1	560	606	0.62(0.07)	3.59(0.29)	5.88(0.65)	-	4.87	1.08
1	560	721	2.26(0.73)	3.38(0.27)	-	-	2.57	1.09
1	635	721	2.51 (1.00)	-	-	-	2.51	1.09

Table S4. Calculation of ETE from fluorescence lifetime.

Compound	λ_{ex}(nm)	λ_{em}(nm)	τ (ns)	ETE = 1- τ_{DA}/τ_{D}
9	440	518	7.93	
6	440	518	0.094	~ 100 %
12	440	518	0.006	~ 100 %
	440	606	4.97	
	560	606	5.95	
1	440	518	0.008	~ 100 %
	440	606	4.23	
	560	606	4.87	~ 18 %

From fluorescence lifetime analysis for RB antenna **6**, energy transfer efficiency (ETE) from Np to aza-BODIPY was calculated to be ~ 100 % in $CHCl_3$ by taking Np compound **9** as the reference energy donor. Similarly for GB antenna **12**, ETE was calculated to be ~ 100 % by taking Np compound **9** as reference energy donor.

For RGB antenna **1**, ETE was calculated to be ~ 100 % from Np to PDI or aza-BODIPY or by cascade way from Np to PDI to aza-BODIPY by taking **9** as reference energy donor and ETE was calculated to be ~ 18 % from PDI to aza-BODIPY by taking GB **12** (λ_{ex} = 560 nm) as reference energy donor.

2.4 Solvatochromism and its influence on energy transfer

The solvatochromism studies of **9**, **6**, **5**, **12** and **1** were performed in five solvents of various polarities in order to assess the possibility of competing electron transfer processes in these molecules and the absorption and emission wavelengths are presented in table S5. Also, energy transfer efficiencies (ETE) were calculated for each compound in these five solvents as presented below in Figures S2-S4 and Table S6.

Table S5. Solvatochromism study of **9**, **6**, **5**, **12** and **1** in different solvents.

Compound	Toluene		$CHCl_3$		THF		DCM		Benzonitrile	
	λ_{abs} (nm)	λ_{em} (nm)	λ_{abs} (nm)	λ_{em} (nm)	λ_{abs} (nm)	λ_{em} (nm)	λ_{abs} (nm)	λ_{em} (nm)	λ_{abs} (nm)	λ_{em} (nm)
9	415	495	430	518	414	514	430	520	430	530
6	430, 695	495, 721	442, 688	494, 717	436, 695	514, 722	440, 688	520, 719	444, 697	530, 728
5	687	713	682	714	687	717	680	712	691	721
12	424, 561	495, 597	436, 564	518, 606	425, 554	490, 592	435, 562	520, 601	440, 566	521, 603
1	427, 565, 701	495, 599, 726 (λ_{exc} = 427 nm)	436, 566, 693	518, 606, 721 (λ_{exc} = 436 nm)	428, 557, 698	482, 596, 725 (λ_{exc} = 428 nm)	440, 563, 691	520, 605, 721 (λ_{exc} = 440 nm)	440, 569, 699	520, 603, 728 (λ_{exc} = 440 nm)

For RB antenna 6

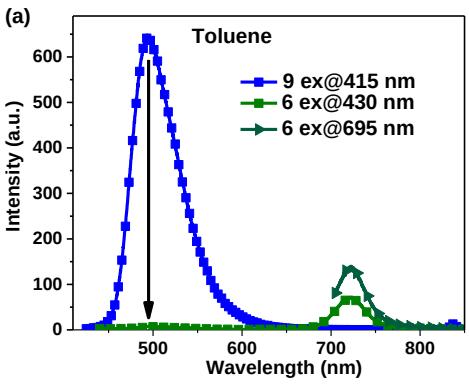

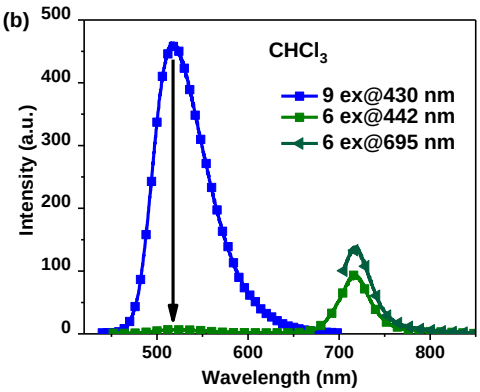

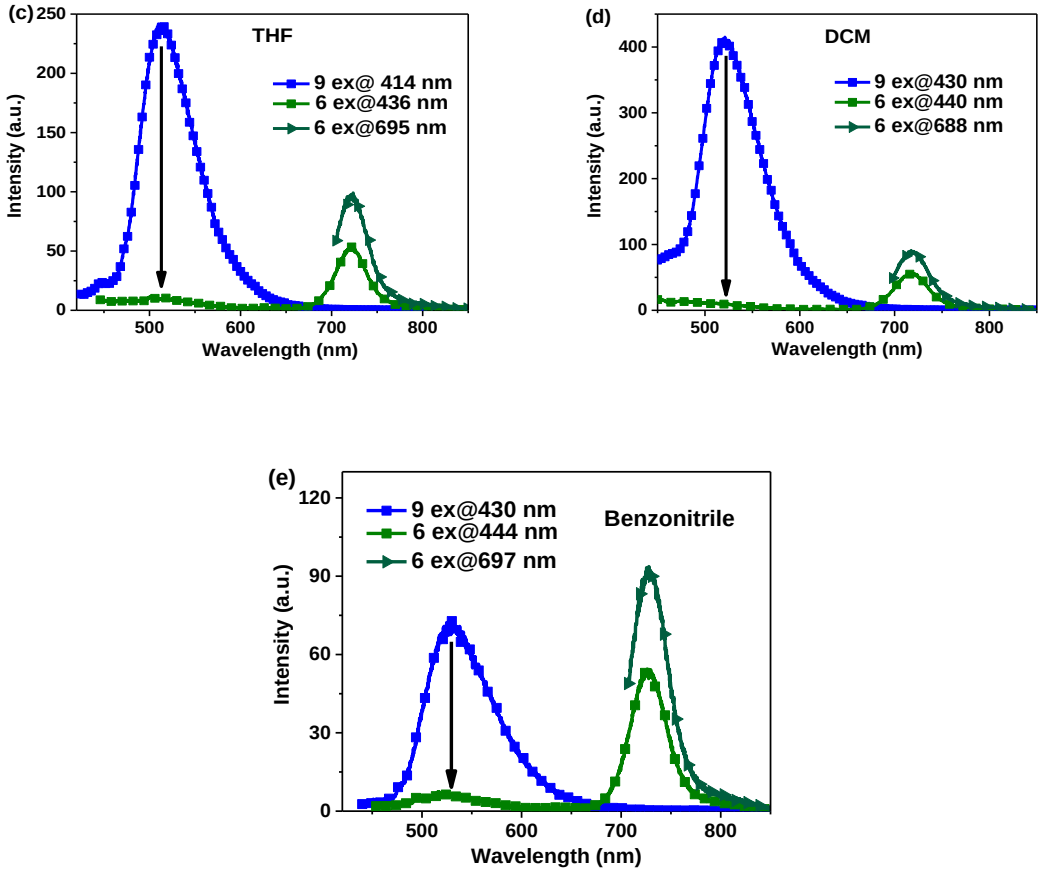

Figure S2. Energy transfer study of RB antenna **6** and its corresponding donor **9** and acceptor **5** in different solvents (a) to (e) ($c \sim 2 \times 10^{-6}$ M).

For GB antenna 12

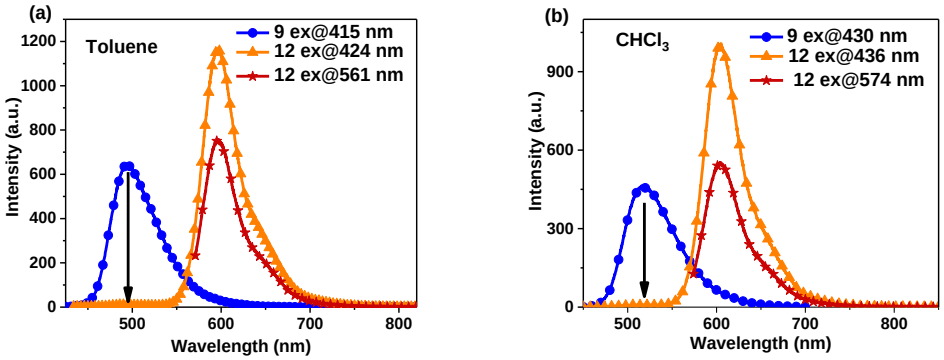

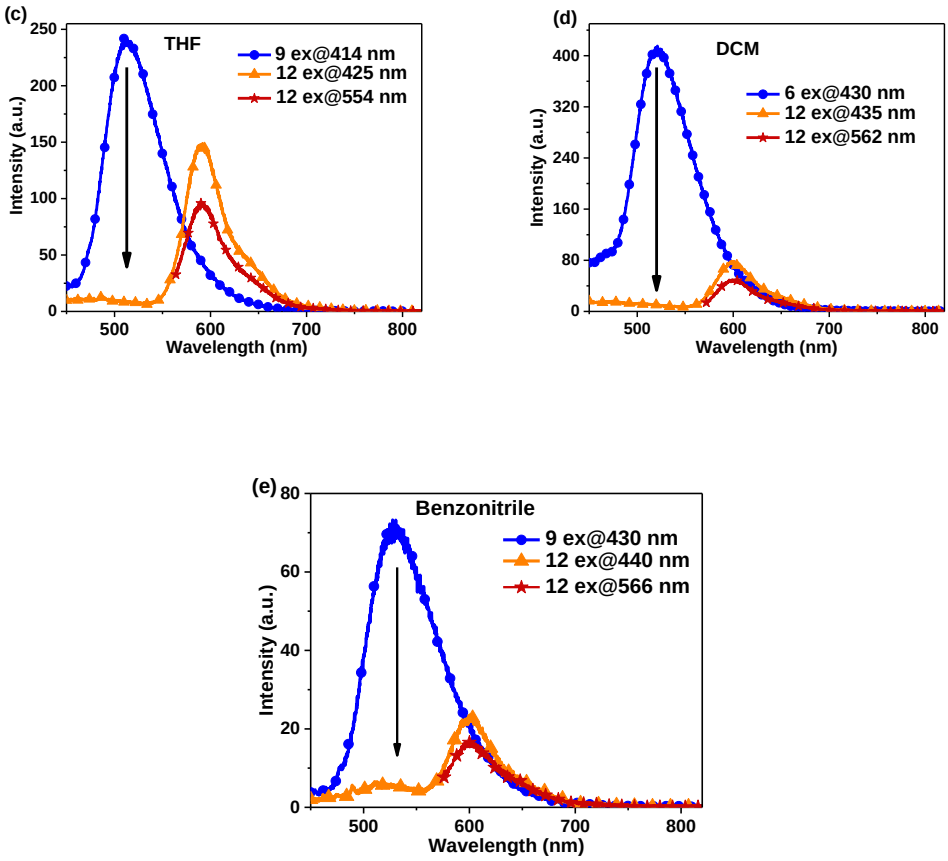

Figure S3. Energy transfer study of GB antenna **12** and its corresponding donor **9** in different solvents (a) to (e) ($c \sim 2 \times 10^{-6}$ M).

For RGB antenna 1

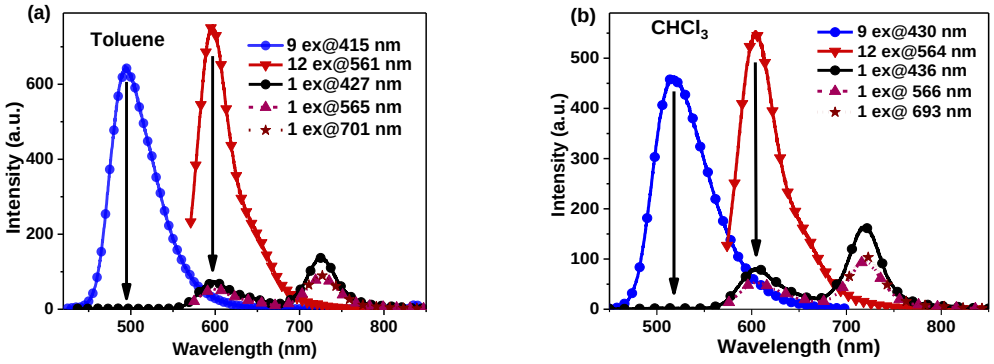

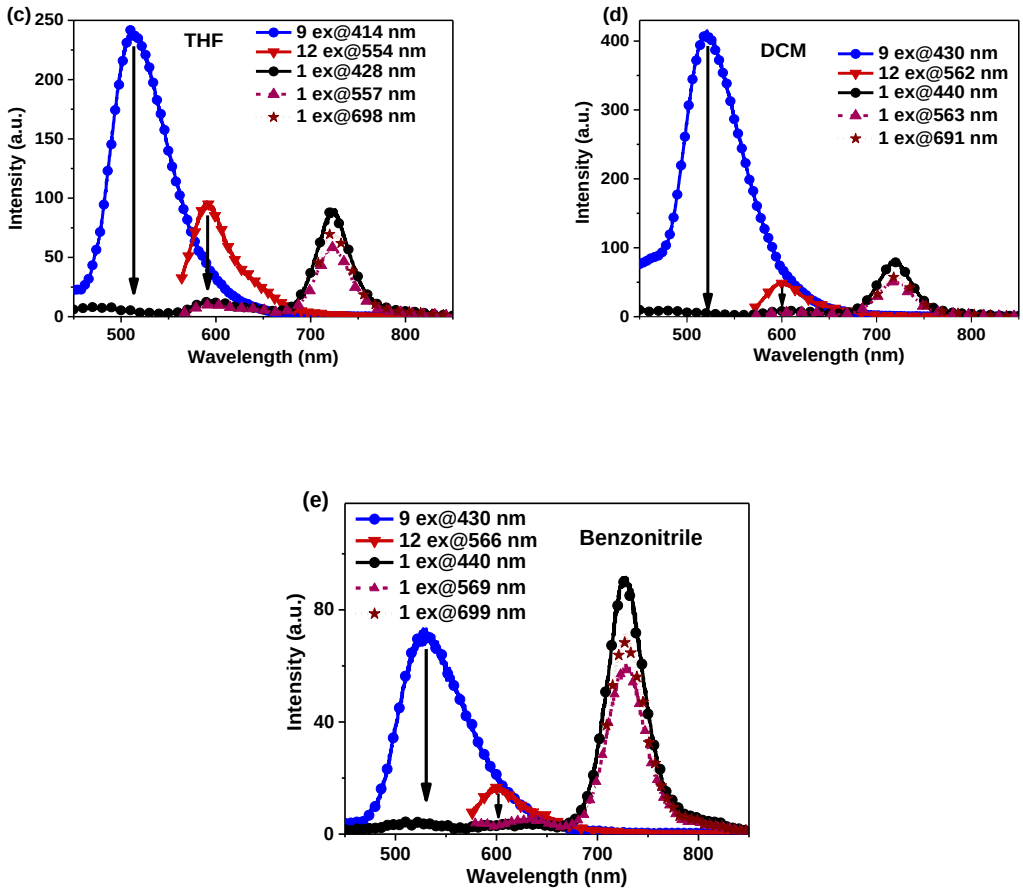

Figure S4. Energy transfer study of RGB antenna **1** and its corresponding subunits donor **9** and GB **12** in different solvents (a) to (e) ($c \sim 2 \times 10^{-6}$ M).

Table S6. Energy transfer efficiencies (ETE) of RB **6**, GB **12** and RGB antenna **1** in different solvents.

Compound		**Toluene**	**$CHCl_3$**	**THF**	**DCM**	**Benzonitrile**
RB 6		~ 99 %	~ 99 %	~ 96 %	~ 98 %	~ 91 %
GB 12		~ 99 %	~ 98 %	~ 96 %	~ 97 %	~ 93 %
RGB 1	**ETE (From Nap)**	~ 100 %	~ 100 %	~ 98 %	~ 99 %	~ 90 %
	ETE (From PDI)	~ 93 %	~ 90 %	~ 90 %	~ 86 %	~ 70 %

The absorption and emission peak maxima for all the model compounds as well as RGB antenna **1** are presented in table S5. Since the absorption and emission peaks maxima for different compounds showing small change in position and not following any trend with polarity, so the solvent polarity has little effect on the ground and excited state properties of all these compounds which further indicates the absence of photoinduced electron transfer

between donor and acceptor components. Further the ETEs were calculated for the model antennae RB **6**, GB **12** and final RGB antenna **1** by comparing the intensities of reference energy donors (F_D) with the decay of donor intensity (F_{DA}) in model as well as RGB antenna **1** according to eq. 1:

$$ETE = 1- F_{DA} / F_D \qquad (1)$$

For antenna RB **6**, on the excitation of donor moiety Np we observed the quenched emission of Np and simultaneous appearance of aza-BODIPY emission, which indicates the energy transfer from Np to aza-BODIPY. However, the acceptor emission intensity it was less compared to direct excitation which could be due to low overlap between Np emission and aza-BODIPY absorption spectrum and other non-radiative quenching pathways like PET from Np to aza-BODIPY (Figure S2a-e). However, solvent polarity dependent emission spectra did not show any strong fluorescence solvatochromism indicating that charge transfer as deactivation pathway is not feasible (Table S5). Furthermore, it is reported that FRET can be observable without spectral overlap of donor emission and acceptor absorption as well as in orthogonally oriented energy donor acceptor systems [S7–S11]. Thus, assuming the major deactivation pathway as energy transfer in case of RB **6**, the calculated ETEs based on quenched emission of donor are shown in table S6.

For antenna GB **12** on excitation at Np absorption, quenching was observed for Np emission and as well as there is enhancement of emission intensity of acceptor on donor excitation compared to direct excitation (Figure S3a-e) which is clear indication of FRET from Np to PDI and calculated ETE s are shown in table S6.

Finally for RGB antenna **1** on excitation at Np (primary donor), the quenching of donor emission was observed in all solvents of various polarity and also the aza-BODIPY (secondary acceptor) emission intensity was increased compared to direct excitation irrespective of the polarity of solvents which clear indicates that FRET is the major deactivation pathway not the electron transfer as electron transfer would have affected the fluorescence spectra by variation of solvent polarity (Figure S4 a-e). On excitation at the PDI (secondary donor) emission intensity of aza-BODIPY in RGB **1** was comparable to direct excitation at aza-BODIPY. The calculated ETEs are shown in table S6.

Also, upon comparing RB **6** and RGB **1**, in case of **1** since the emission intensity of aza-BODIPY secondary acceptor enhanced on Np excitation compared to direct excitation, but in **6** emission intensity of aza-BODIPY acceptor was less on Np excitation compared to direct excitation which confirms that energy transfer occurs via cascade way from Np to PDI to aza-BODIPY in RGB **1**.

3. Ratiometric temperature sensing

For ratiometric analysis for RB antenna **6** in $CHCl_3$ (graph shown in the main text; figure 3a), the plot of intensity ratio of two emissions at Np channel and PDI channel were plotted with

temperature (i.e., plots of $I_1/(I_1 + I_2)$ vs. temperature; figure 3b) and fitted with a linear function with goodness of fit ($R^2 = 0.97$) and the fitted equation was given by eq. (2):

$$I_{518}/(I_{518} + I_{717}) = 0.00095T + 0.057 \quad (2)$$

The plot of intensity ratio with temperature of GB antenna **12** (figure 3d) in $CHCl_3$ was fitted exponentially and slope of exponential fit[S12] is the internal sensitivity (Figure S5) and obtained by differentiating the $I_1 / I_1 + I_2$ vs T fitted curve according to eq. (3):

$$S_{int}(T) = |\partial(I_1/(I_1+I_2))/\partial T| \quad (3)$$

and temperature sensitivities varied from 0.015 % $°C^{-1}$ (at -10 °C) to 0.001 % $°C^{-1}$ (at 60 °C) for GB antenna **12**.

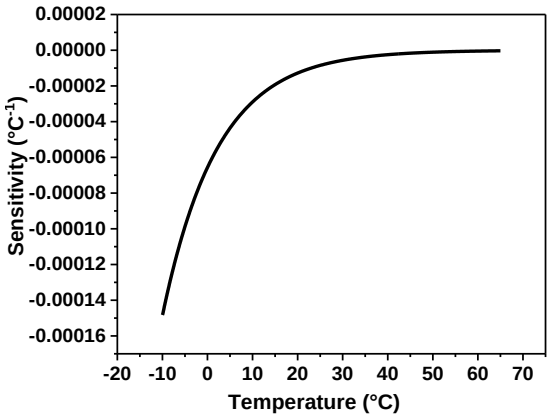

Figure S5. The temperature sensitivity of GB **12**.

The plot of intensity ratio with temperature of RGB antenna **1** (Figure 3f)in $CHCl_3$ was fitted with a linear function (goodness of fit $R^2 = 1$) was given by eq. (4):

$$I_{606}/(I_{606} + I_{721}) = 0.0041T + 0.215 \quad (4)$$

The temperature-dependent absorption spectra of RB **6**, GB **12** and RGB antenna **1** showed negligible decrease in absorbance while increasing temperature from 10 ^oC to 50 ^oC (Figures S6 a-c).

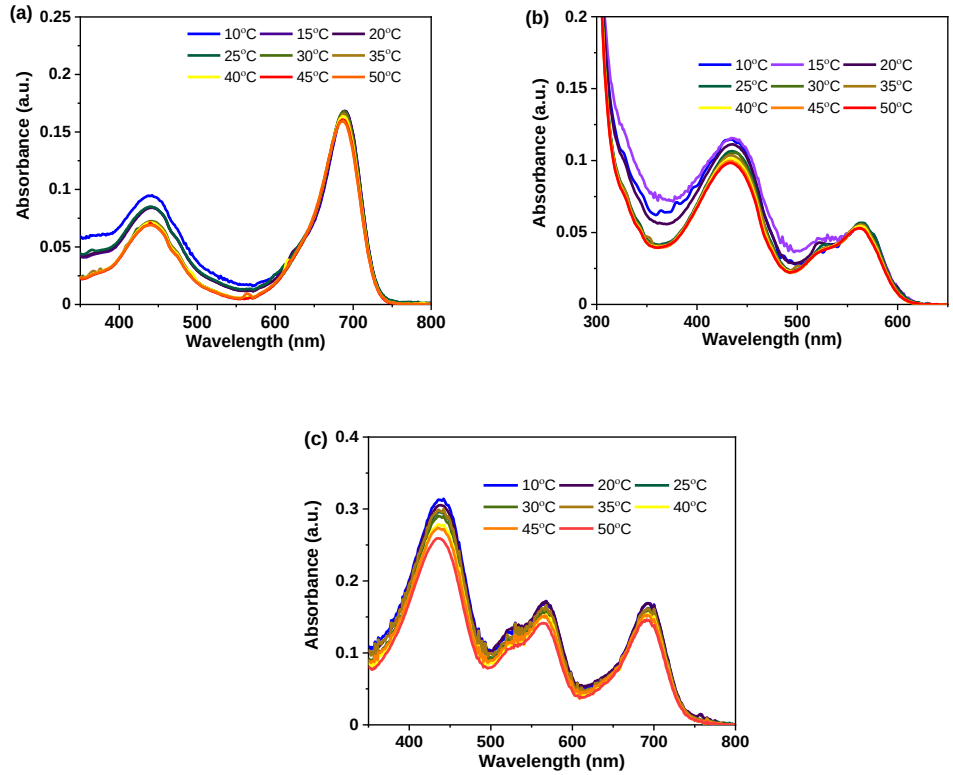

Figure S6. Temperature-dependent absorption spectra of (a) RB **6** and (b) GB **12** and (c) RGB antenna **1** in $CHCl_3$.

4. Electrochemical properties

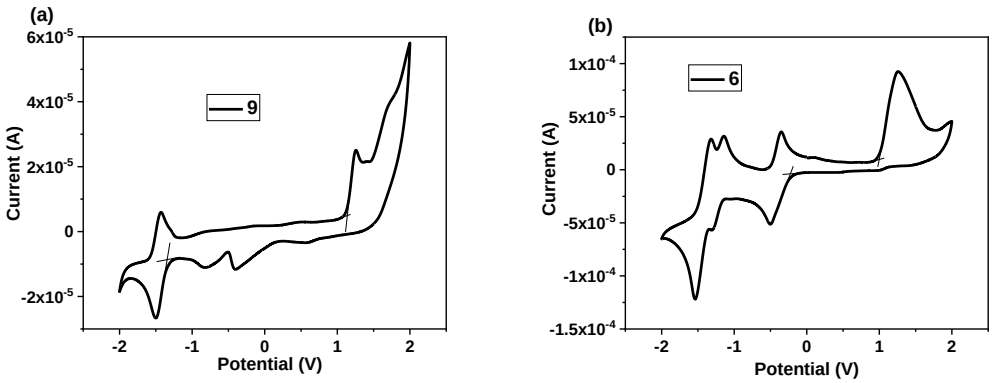

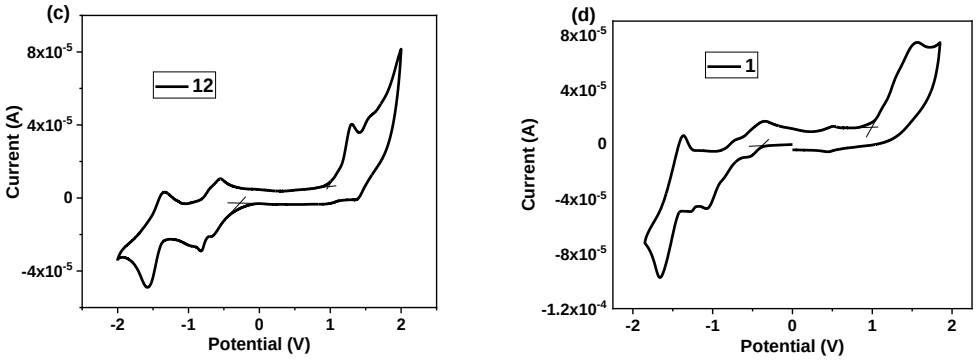

Figure S7. The cyclic voltammograms of (a) **9**, (b) RB **6**, (c) GB **12** and (d) RGB antenna **1** in dry DCM with 0.1 M tetrabutyl ammonium hexafluorophosphate (TBAHFP) as supporting electrolyte at *c* ~ 0.5 mM VS Ag/AgCl reference electrode at scan rate of 0.1 V/s.

The cyclic voltammogram of Np **9**, RB **6**, GB **12** and RGB antenna **1** were recorded in DCM in order to understand their redox behavior and calculate their frontier molecular orbital energy levels (Figure S7). The cyclic voltammogram of naphthalimide reference compound **9** showed one reversible reduction peak at -1.46 V and one irreversible oxidation peak at +1.25 V (Figure S7 (a)). RB **6** showed first and second reversible reduction waves at -0.43 V and -1.23 V for two reversible reductions of aza-BODIPY part and third reduction at -1.43 V for Np reduction part and in oxidation side it showed one irreversible oxidation wave at +1.25 V for Np part (Figure S7 (b)). For GB **12**, cyclic voltammogram showed two reversible reduction waves at -0.61 V and -0.76 V for first and second reduction of PDI and third reduction wave at -1.46 V for Np moiety. On oxidation side, there was one irreversible oxidation wave at +1.31 V for Np and second reversible oxidation peak at +1.46 V for PDI part (Figure S7 (c)). RGB antenna **1** showed first reversible reduction at -0.45 V for aza-BODIPY first reduction, second reversible peak at -0.78 V for first reduction of PDI, peaks at -1.08, -1.28 for the second reduction of PDI and aza-BODIPY respectively and reduction at -1.52 V for Np reduction (Figure S7 (d)). The HOMO/LUMO alignment for all compounds are shown in Figure S8.

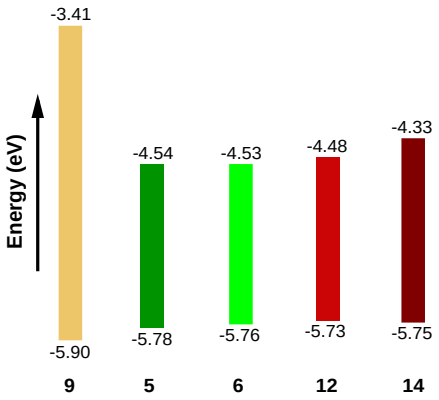

Figure S8. Alignment of frontier molecular orbital energy levels (in eV) obtained from cyclic voltammetry measurements for **9**, **5**, RB **6**, GB **12** and RGB **1**.

5. Spectroelectrochemistry

For all compounds, spectrochemical measurements were performed as described in the materials and methods section and for clarity, spectral changes in the forward oxidation cycle (voltage sweep in 0 to +2 V range) only are shown. Similarly, spectral changes in the forward reduction cycle (0 to -2 V) are shown for clarity for each compound. It is to be noted that the spectral changes were completely reversible upon sweeping the voltage in the opposing direction in each case of oxidation or reduction.

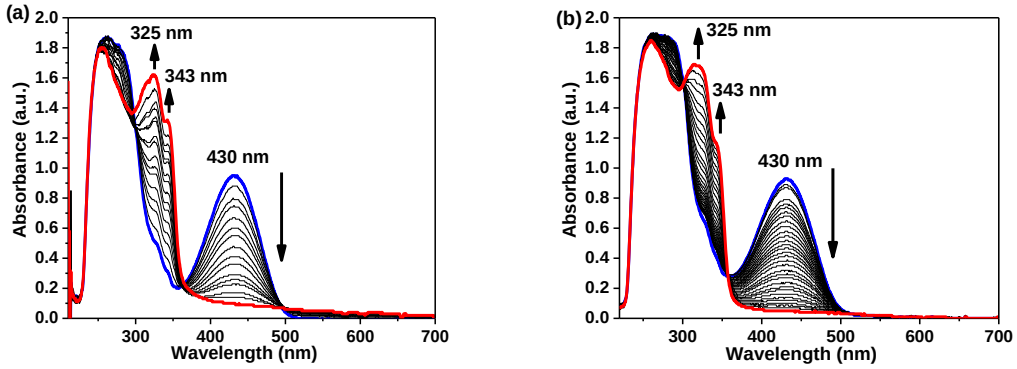

Figure S9. Spectroelectrochemical changes observed for Np compound **9** during (a) Oxidation and (b) Reduction process. Initial and final spectra are represented by blue and red respectively.

The Np compound **9** showed depletion of main absorption band at 430 nm and two new bands emerged at 325 nm and 343 nm during both oxidation and reduction indicative of the fact that both $Np^{+\cdot}$ And $Np^{-\cdot}$ are characterized by depletion of main band and emergence of two new bands (Figure S9) in the UV region.

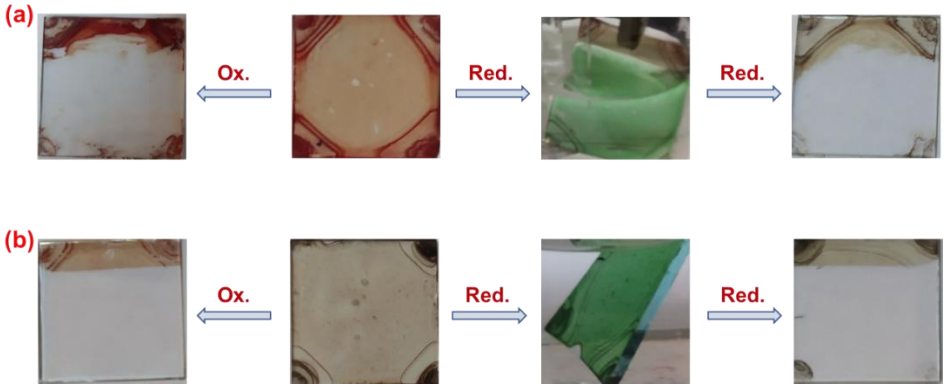

Figure S10. Colour change upon oxidation and reduction cycle on (a) GB **12** and (b) RGB antenna **1** coated on ITO substrate.

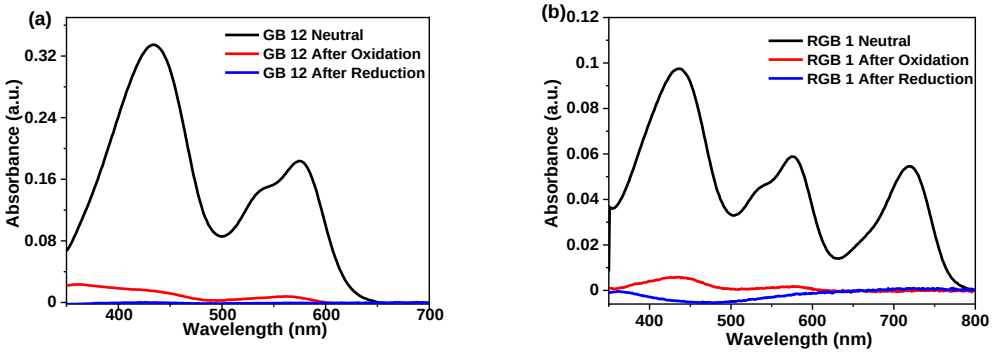

Figure S11. UV/Vis absorption spectra of (a) GB **12** and (b) RGB antenna **1** films on ITO substrate upon oxidation and reduction.

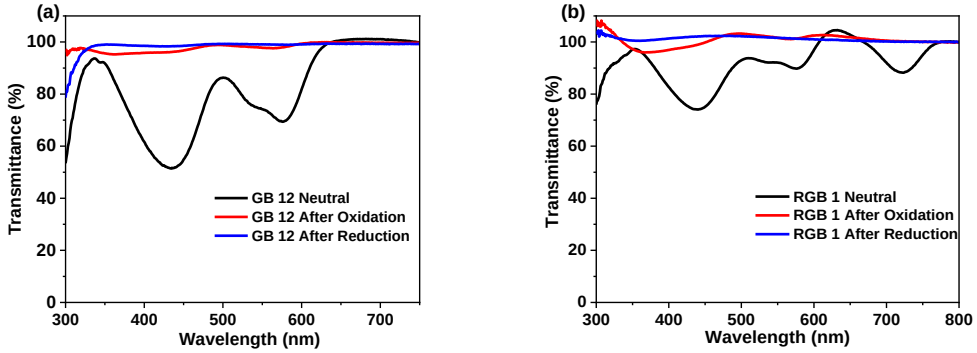

Figure S12. Transmittance spectra of (a) GB **12** and (b) RGB antenna **1** films on ITO substrate upon oxidation and reduction.

6. Acid Base Sensing

Acid base sensing experiments were performed for all compounds (c ~ 5μM) by adding sequentially increasing amounts of trifluoroacetic acid (TFA) and recording UV/Vis and emission spectra after every equivalent addition. Subsequently, the solutions were back titrated with increasing amount of triethylamine (TEA) with concurrent UV/Vis and fluorescence emission spectra measurement after every equivalent addition of TEA.

For RB antenna 6

RB antenna **6**, with the addition of TFA the absorbance of naphthalimide band decreased (Figure 6c in main paper) and aza-BODIPY band was blue shifted (colour of RB **6** changed from yellowish green to green) while on back titrating with TEA, absorbance of naphthalimide was regenerated and aza-BODIPY band was red shifted (Figure S13a) (colour changed from green to yellowish green). In case of emission spectra (λ_{ex} = 396 nm), upon titration with TFA, fluorescence intensity of both naphthalimide and aza-BODIPY decreased (Figure 6d in main paper) and on back titration with TEA intensity was again recovered (Figure S13b). Similar trend was observed on excitation at 442 nm (Figure S14c-d). In case of 688 nm excitation the

fluorescence intensity of aza-BODIPY band was increased as well as blue shifted and on back titration it was decreased and red shifted (Figure S15e-f).

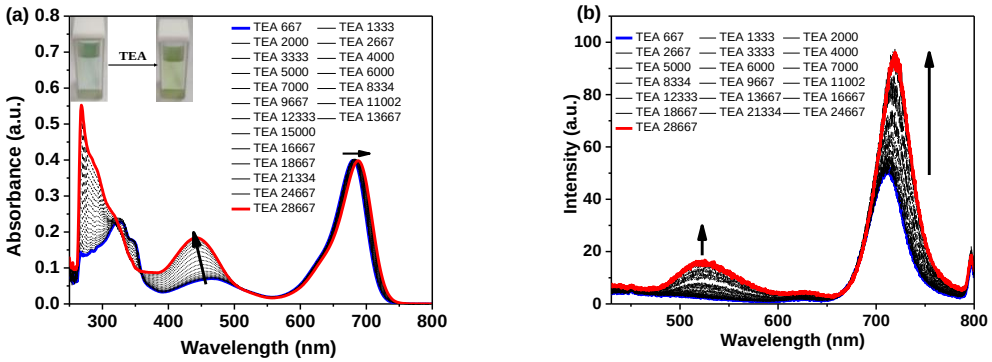

Figure S13. Change in absorption and emission (λ_{ex} = 396 nm) (a) and (b) spectra of RB antenna **6** on back titration with TEA in $CHCl_3$ (Blue represents the initial spectrum and red represents the final spectrum).

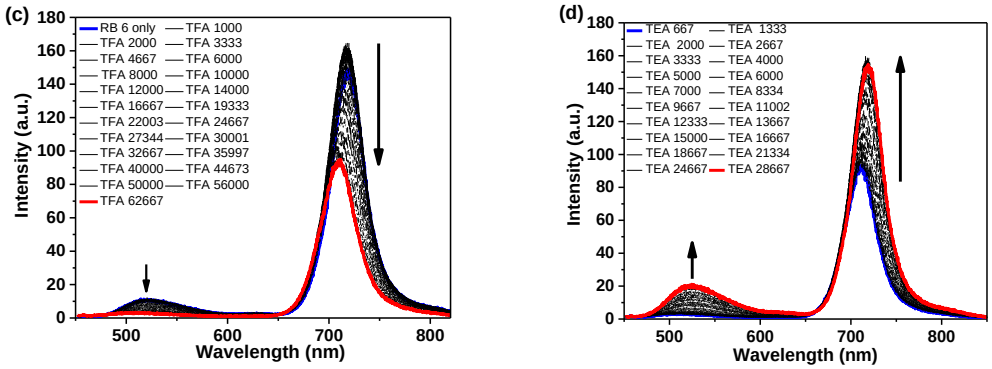

Figure S14. Change in emission (λ_{ex} = 442 nm) spectra (c) and (d) of RB antenna **6** on titration with TFA and back titration with TEA in $CHCl_3$ (Blue represents the initial spectrum and red represents the final spectrum).

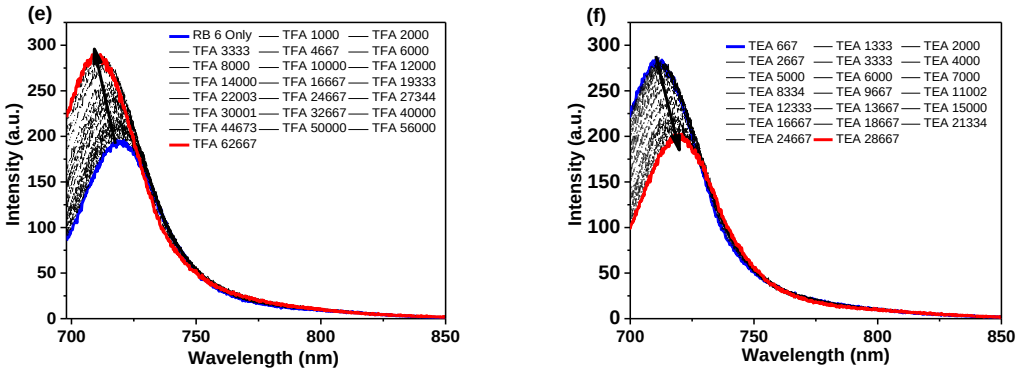

Figure S15. Change in emission (λ_{ex} = 688 nm) (e) and (f) of RB antenna **6** on titration with TFA and back titration with TEA in $CHCl_3$ (Blue represents the initial spectrum and red represents the final spectrum).

For GB antenna 12

GB antenna **12**, on titration with TFA the absorption band corresponding to Np band depleted (colour of the GB **12** changed from red to pink) (Figure S16a) and PDI band was little red shifted while on back titration with TEA Np band was recovered back (colour changed from pink to reddish) and PDI band was blue shifted (Figure S16b).

On titration with TFA for GB **12** (λ_{ex} = 436 nm), the emission intensity of PDI band decreased drastically up to 38000 equivalents of TFA and on further addition of TFA intensity increased as well as red shifted (Figure S17c). Further on back titration with TEA, intensity was further decreased up to 13000 equivalents and then increased (Figure S17d). For 564 nm excitation, the intensity of PDI band decreased drastically up to 28005 equivalents of TFA and on further addition of TFA, emission intensity increased as well as red shifted (Figure S18e). Further on back titration with TEA intensity has further decreased (Figure S18f).

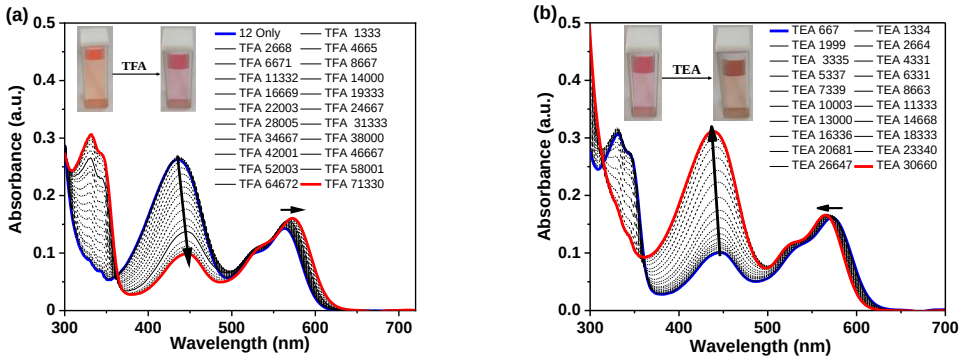

Figure S16. Change in absorption (a) and (b) spectra of GB antenna **12** on titration with TFA and back titration with TEA in $CHCl_3$ (Blue represents the initial spectrum and red represents the final spectrum).

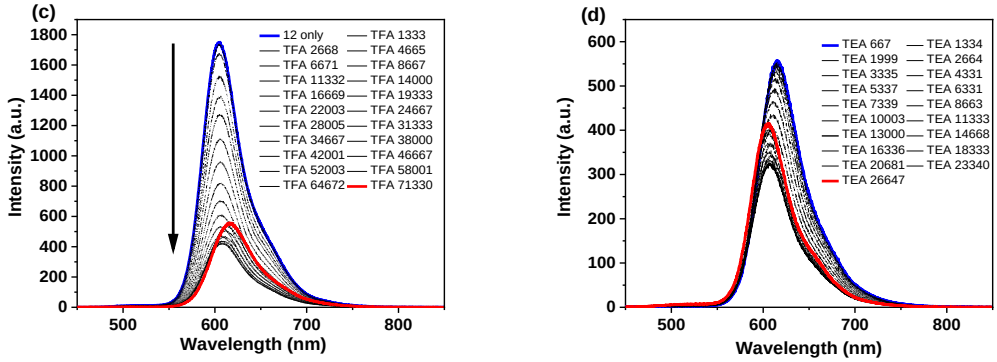

Figure S17. Change emission (λ_{ex} = 436 nm) (c) and (d) spectra of GB antenna **12** on titration with TFA and back titration with TEA in $CHCl_3$ (Blue represents the initial spectrum and red represents the final spectrum).

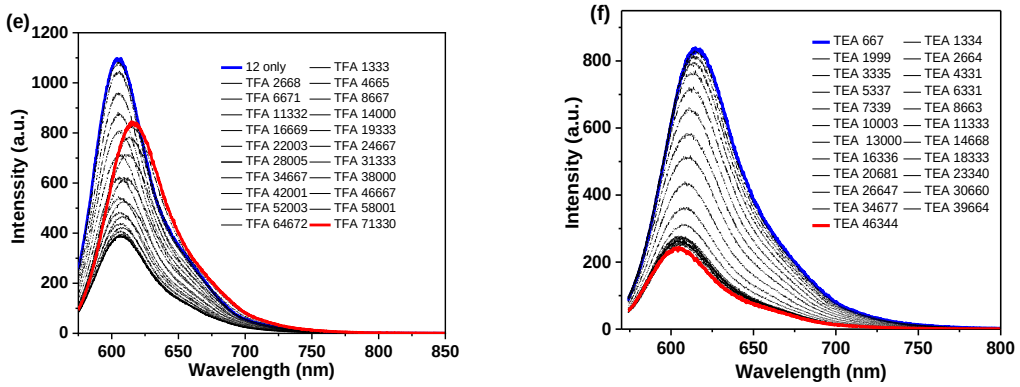

Figure S18. Change emission (λ_{ex} = 564 nm) (c) and (d) spectra of GB compound **12** on titration with TFA and back titration with TEA in $CHCl_3$ (Blue represents the initial spectrum and red represents the final spectrum).

For RGB antenna 1

RGB antenna **1** showed the cumulative effect on addition of acid and base as observed for the effect of acid and base in the constituent subchromophoric units. RGB antenna **1** on titration with TFA showed the depletion of Np absorption band and PDI band showed minimal red shift while aza-BODIPY band blue shifted (Figure 6a in main paper) and on back titration with TEA, Np absorbance recovered to its original value, PDI and aza-BODIPY shifted minimally to blue and red wavelengths respectively (Figure S19a).

Upon 396 nm excitation (where selectively the Np absorbs and there is no absorbance of aza-BODIPY) and measurement of fluorescence with titration with TFA, the fluorescence intensities of both PDI and aza-BODIPY decreased and it could be attributed to depletion of Np band absorbance which leads to decrease in spectral overlap between the Np and PDI/aza-BODIPY therefore FRET from Np to PDI or aza-BODIPY has decreased (Figure 6b in main paper). Upon titration with TEA, intensity of aza-BODIPY was recovered while intensity of PDI band first decreased and blue shifted up to 13000 equivalents of TEA and on further addition of TEA it has increased (Figure S19b).

Upon 436 nm excitation (major absorption of Np but some absorption contribution from aza-BODIPY), the intensity of PDI band was first decreased up to 30667 equivalents of TFA and then started increasing and for aza-BODIPY band, the intensity first increased and blue shifted up to 40667 equivalents and then started decreasing (Figure S20c) and on back titration with TEA the intensity of aza-BODIPY band decreased and that of PDI band first decreased up to 19000 equivalnts and on further addition intensity has increased (Figure S20d).

Further at 566 nm excitation at PDI band on acid addition the intensity of aza-BODIPY band has increased, for PDI band drastically decreased up to 30667 TFA equivalents and further addition of acid led to increase in intensity of PDI band (Figure S21e). Further on back titration with TEA, the intensity of aza-BODIPY band was decreased and that of PDI band first decreased drastically up to 19000 TFA equivalents and then it was increasing (Figure S21f).

On excitation at 693 nm (aza-BODIPY absorption) on acid addition, the intensity of aza-BODIPY was increased (Figure S22g) and on back titration it was decreasing (Figure S22h).

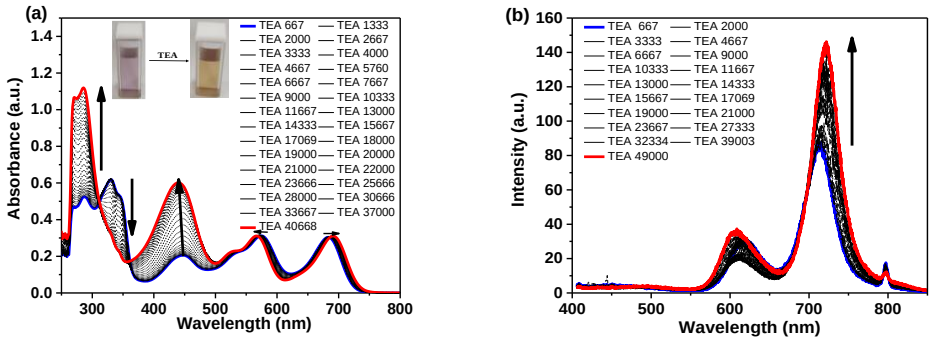

Figure S19. Change in absorption and emission (λ_{ex} = 396 nm) (a) and (b) spectra of RGB antenna **1** on back titration with TEA in $CHCl_3$ (Blue represents the initial spectrum and red represents the final spectrum).

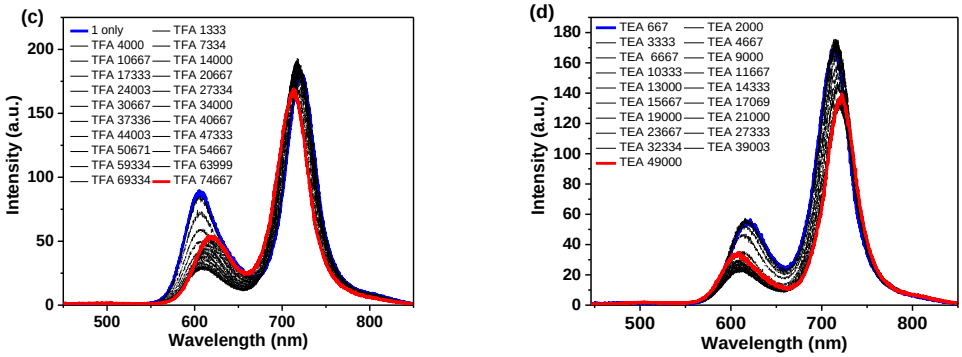

Figure S20. Change in emission (λ_{ex} = 436 nm) spectra (c) and (d) spectra of RGB antenna **1** on titration with TFA and back titration with TEA respectively in $CHCl_3$ (Blue represents the initial spectrum and red represents the final spectrum).

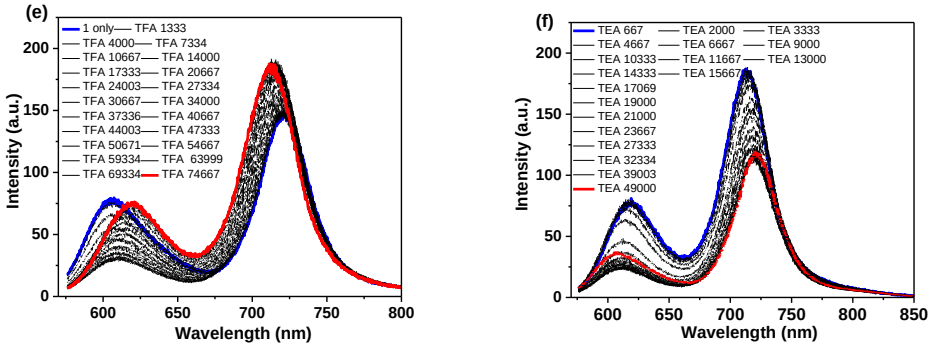

Figure S21. Change in emission (λ_{ex} = 566 nm) spectra (e) and (f) spectra of RGB antenna **1** on titration with TFA and back titration with TEA respectively in $CHCl_3$ (Blue represents the initial spectrum and red represents the final spectrum).

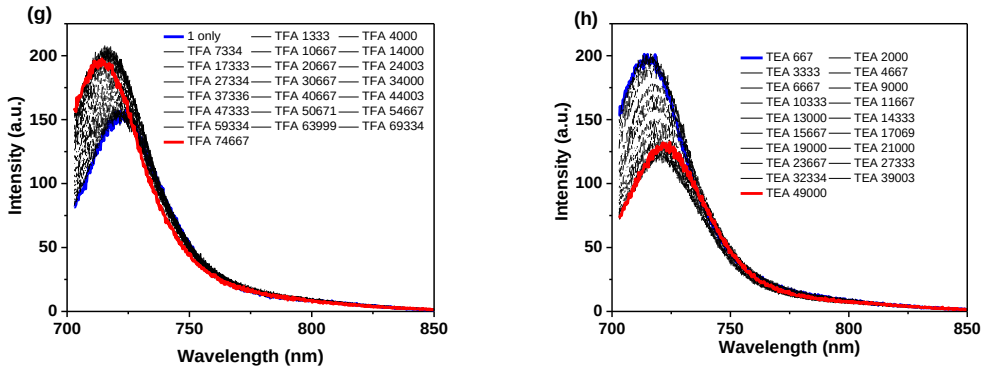

Figure S22. Change in emission (λ_{ex} = 693 nm) spectra (e) and (f) spectra of RGB antenna **1** on titration with TFA and back titration with TEA respectively in $CHCl_3$ (Blue represents the initial spectrum and red represents the final spectrum).

pH sensing in THF/H_2O mixture

The pH sensing experiments of RB **6**, GB **12** and RGB **1** were performed in semi-aqueous solvent mixture i.e., THF/aqueous buffer mixture due to insolubility of these antennae compounds in pure water.[S13] In THF/aqueous buffer mixture RB **6** and GB **12** antennae showed slight red shift of ~25 nm and RGB **1** showed red shift of ~40-49 nm compared to pure THF due to the aggregate formation and the emission intensity was quenched. The pH of the solutions were varied and adjusted by adding diluted TFA in the aqueous buffer solution in the THF/aqueous buffer mixture.

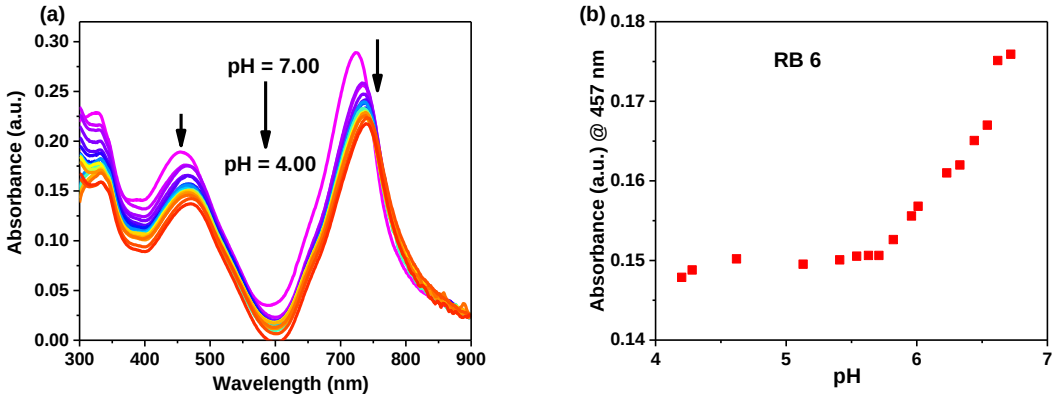

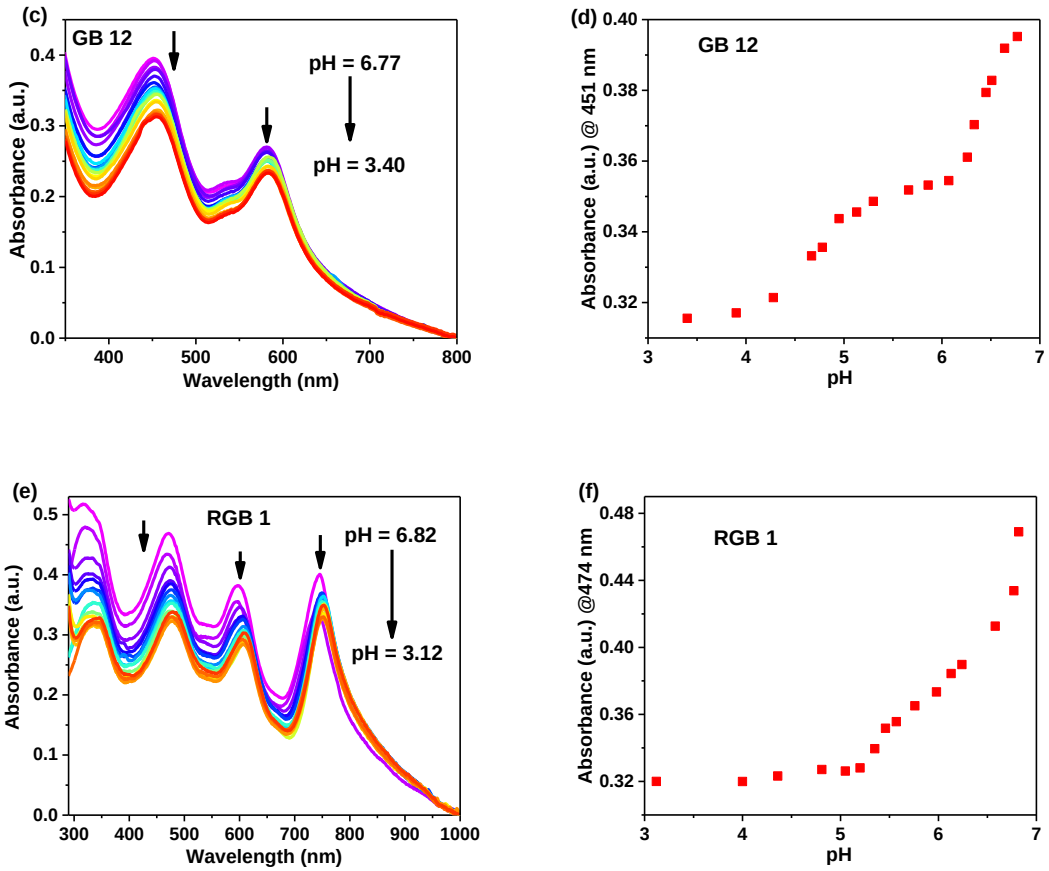

Figure S23. The pH-dependent UV/Vis titration spectra and the plot of absorbance vs pH (a) and (b) RB **6**; (c) and (d) GB **12**; (e) and (f) RGB **1** in 25/75 THF/aqueous buffer; (compound, *c* ~ 5 μM).

Upon decreasing the pH from 7 up to 5.71, antenna RB **6** showed the decrease in Np absorption band at 457 nm along with slight bathochromic shift and upon further decrease in pH it was constant. Aza –BODIPY band at 725 nm also showed decrease in absorbance upon decrease in pH (Figure S23a-b) though the changes were less pronounced. GB antenna **12** also showed depletion of Np band at 451 nm upon decreasing the pH from 7 to 4.28 then it became constant with further decrease in pH (Figure S23c-d).

For RGB **1**, with the decrease in pH from 7 to 5.20, the absorbance of Np band decreased as well as red shifted (Figure S23e). The PDI and aza-BODIPY bands also showed depletion upon decrease in pH, but the decrease in the absorbance at Np band was more pronounced compared to PDI and aza-BODIPY band due to the protonation at amine Nitrogen atom, hence loss of conjugation led to decrease in absorbance of Np. The corresponding graph for change in absorbance at 474 nm vs pH is shown in figure S23f.

7. Spectral properties in thin films

Thin films of RB **6**, GB **12** and RGB **1** were prepared by drop-casting the $CHCl_3$ solutions of corresponding compounds on to quartz substrates and UV/Vis spectra were recorded; PDI (~10 nm) and aza-BODIPY (~25 nm) bands get red shifted while Np band remained unaffected (Figure S24).

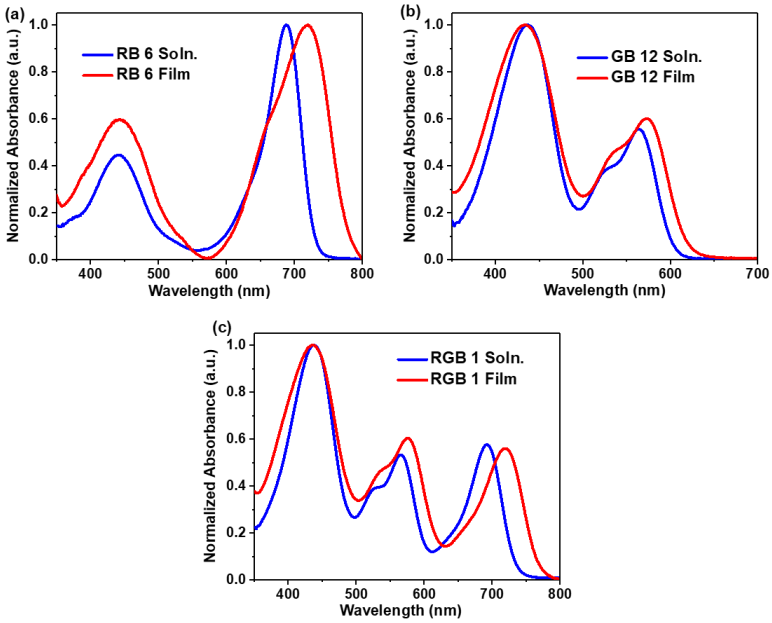

Figure S24. Thin Film UV/Vis spectra of RB **6**, GB **12** and RGB antenna **1**.

Furthermore, thin films of RGB **1** and RB **6** showed reversible colour change upon exposure to TFA vapours and colour is coming back to original colour after some time due to TFA evaporation and thus serve as vapor sensitive solid-state sensors (Figure S25).

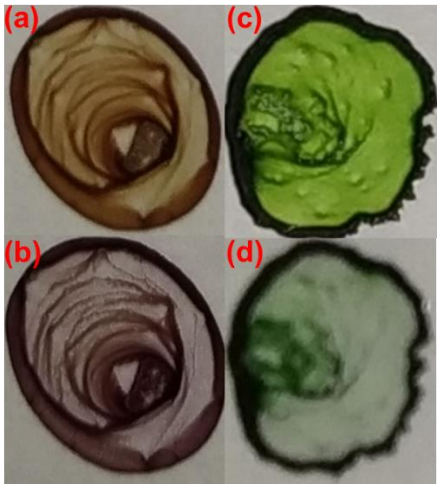

Figure S25. Change in colours of thin films of (a), (b) RGB **1** and (c), (d) RB **6** on exposure to TFA vapours.

8. Metal ion sensing

Metal ion sensing experiments were performed first by screening with different metal ions, compound and metal ion stock solutions were prepared in THF, then compound solution was

diluted to 5 μM to which 20 equiv. of metal ion solution was added, samples were kept overnight and UV/Vis and emission spectra for all samples were recorded.

For RGB antenna compound 1

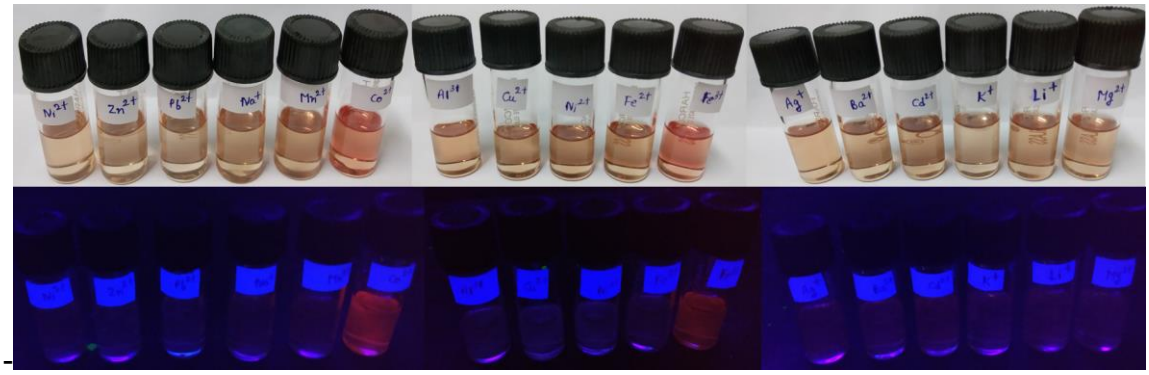

Figure S26. Photographs of RGB antenna **1** solutions with addition of different cations under normal light (top) and under UV light (bottom). Only the solutions with Co^{2+} and Fe^{3+} showed visual colour change under normal light or under UV light.

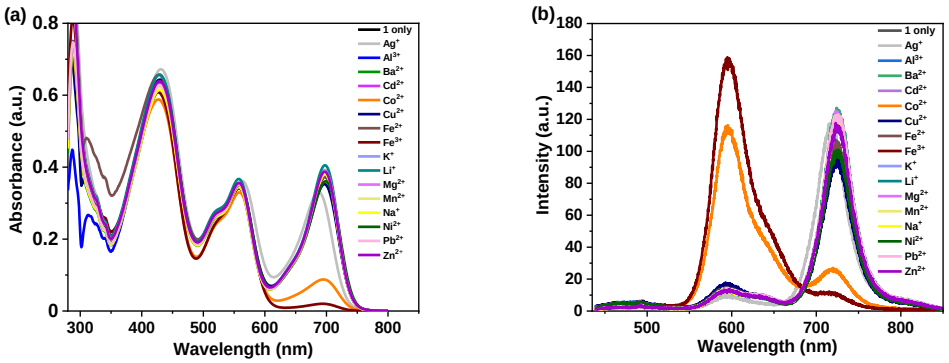

Figure S27. (a) Changes in absorption and (b) fluorescence spectra of RGB antenna **1** (*c* ~5 μM) upon addition of different metal ions (20 equiv.) in THF solution.

On screening with multiple metals it was observed that RGB antenna **1** was highly sensitive to Co^{2+} and Fe^{3+} metal ions (colour was changed from brownish to dark red; Figure S26), in absorption spectrum the aza-BODIPY band got depleted (Figure S27a) which led to decrease in spectral overlap between the energy donor PDI and aza-BODIPY acceptor (Figure S27b), thus turning off the FRET between PDI and aza-BODIPY. As a result of FRET turn off, the intensity of PDI band increased by 11 % for Co^{2+} and 12 % for Fe^{3+} and intensity ratio (I_{595}/I_{725}) increased from 0.103 to 4.52 for Co^{2+} and 0.103 to 16.06 for Fe^{3+}.

Association constant (K_a)

The association constant (K_a) for metal ions with different compounds were calculated according to earlier reported Merkx model.[S14] Merkx model works well for FRET systems that show multiple emission bands with pronounced isosbestic points and it has several advantages

over the other commonly used Krężel model.[S15] Krężel model gave different results of association constants in the two different fits ($R_{1/2}$ vs $[L_u]$ or $R_{2/1}$ vs $[L_u]$) where $R_{1/2}$ indicates ratio of fluorescence intensities at donor and acceptor emission wavelengths and $[L_u]$ the concentration of unbound ligand. A correction was provided by the Merkx model that used the fluorescence intensity at the isosbestic point and therefore it acts like an internal calibration.[S14] Utilizing the Merkx model yields uniform and similar K_d values both from the $R_{donor/isosbestic}$ or $R_{acceptor/isosbestic}$,[S14] and their average can be taken as the K_d value for the system. Since Merkx model works best for systems with multiple emissions with isosbestic points, we have used the model to calculate the association constants for the interaction of Co^{2+} and Fe^{3+} (Figure S28 and S29) with RB **6** and RGB antenna **1**.

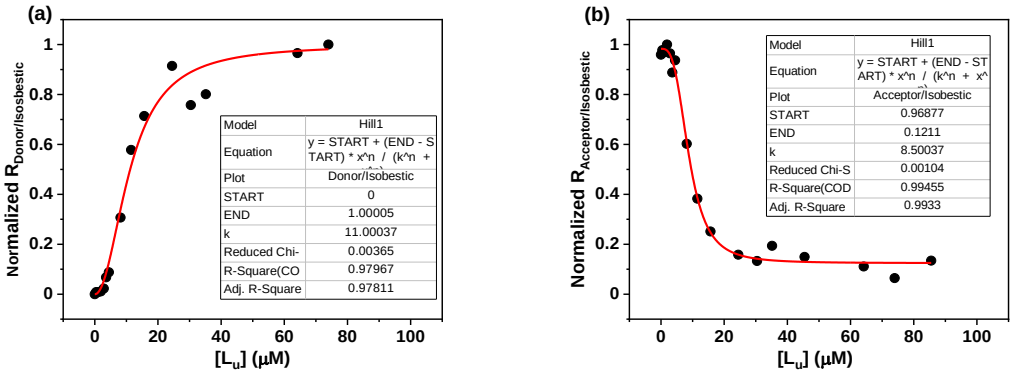

Figure S28. Normalized (a) $R_{donor/isosbestic}$ plot with concentration of unbound guest, (b) Normalized $R_{acceptor/isosbestic}$ plot with concentration of unbound guest using Merkx model for determination of association constant of RGB antenna **1** with Co^{2+}.

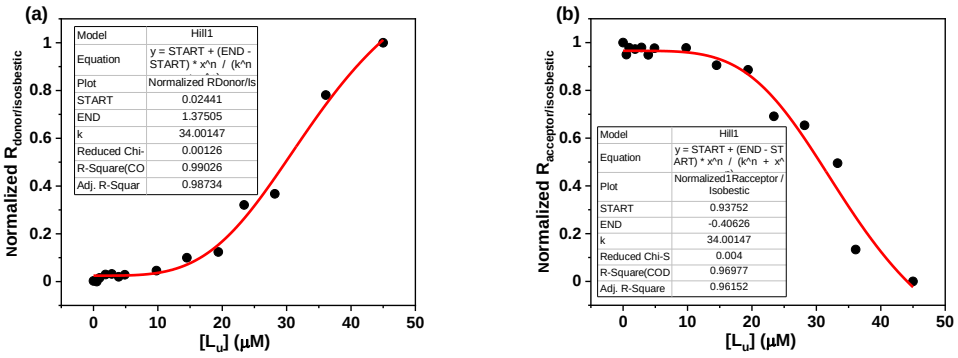

Figure S29. Normalized (a) $R_{donor/isosbestic}$ plot with concentration of unbound guest, (b) Normalized $R_{acceptor}/_{isosbestic}$ plot with concentration of unbound guest using Merkx model for determination of association constant of RGB antenna **1** with Fe^{3+}.

Job's plot

In order to assess the stoichiometry of metal and compound, the method of continuous variation or Job's plot was adopted. Different samples were prepared from compound and metal stock by fixing total concentration as 10 μM.

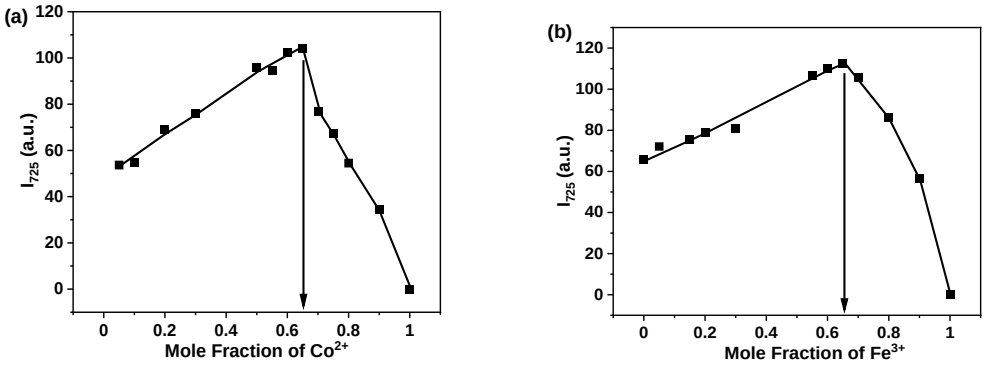

Figure S30. Job's plots for RGB antenna **1** with (a) Co^{2+} and (b) Fe^{3+} in THF according to aza-BODIPY emission respectively. The total concentration of [Co^{2+}] / [Fe^{3+}] and **1** is 10 μM.

The RGB antenna **1** was photoexcited at 430 nm and the intensity of the aza-BODIPY fluorescence (I_{725}) was plotted against the mole fraction of the metal cation for every solution and the Job's plots showed an inflexion point (intersection of the fitted lines of the two sets of data points) at a value of ~ 0.67 that revealed a stoichiometry of 1:2 for **1** with Co^{2+} and Fe^{3+} (Figure S30).

For RB antenna 6

For RB **6**, the metal sensing was performed with Co^{2+} and Fe^{3+} as of RGB antenna **1**, it showed the depletion of aza-BODIPY band with the addition of these metals, as a result the spectral overlap between Np and aza-BODIPY became negligible, thus turning off the FRET process between Np and aza-BODIPY. The FRET turn-off led to the enhancement of fluorescence intensity of Np band by 44 % for Co^{2+} and by 58 % for Fe^{3+} (Figure S31 and S33). The intensity ratio (I_{518}/I_{725}) increased from 0.065 to 19.38 for Co^{2+} and from 0.06 to 291.34 for Fe^{3+}.

The association constant of RB **6** with Co^{2+} and Fe^{3+} were determined by above described Merkx model (Figure S32 and S34) and values are depicted in table S8.

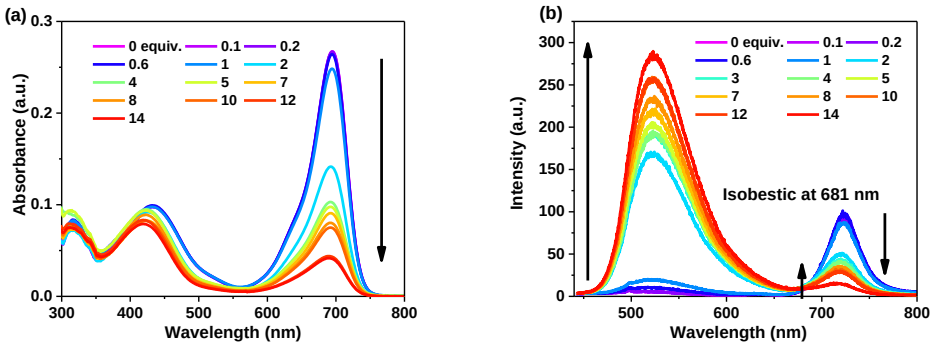

Figure S31. Change in (a) absorption and (b) emission (λ_{ex} = 433 nm) spectra of RB antenna **6** on titration with increasing equivalents of Co^{2+} in THF.

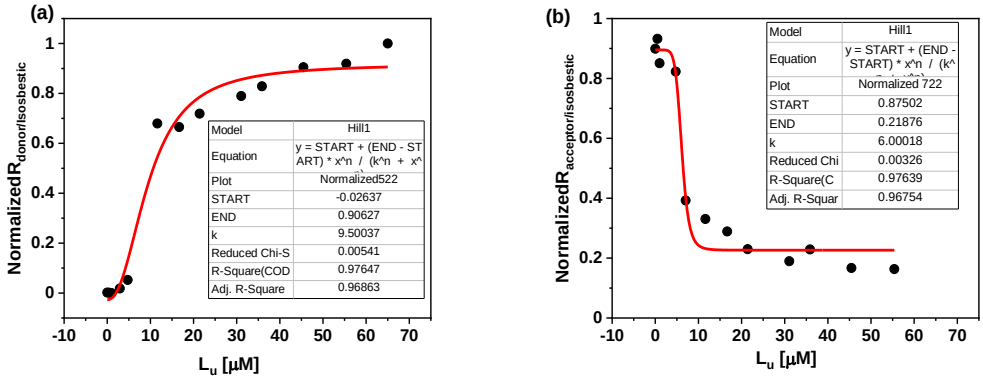

Figure S32. Normalized (a) $R_{donor/isosbestic}$ plot with concentration of unbound guest, (b) Normalized $R_{acceptor/isosbestic}$ plot with concentration of unbound guest using Merkx model for determination of association constant of RB antenna **6** with Co^{2+}.

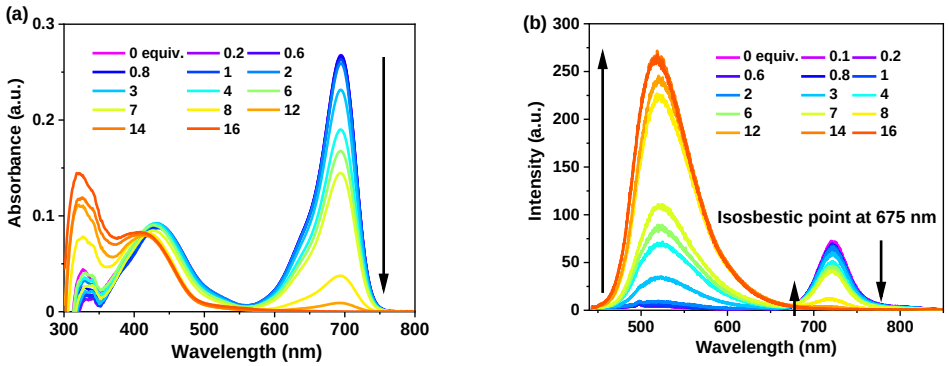

Figure S33. Change in (a) absorption and (b) emission (λ_{ex} = 433 nm) spectra of RB antenna **6** on titration with increasing equivalents of Fe^{3+} in THF.

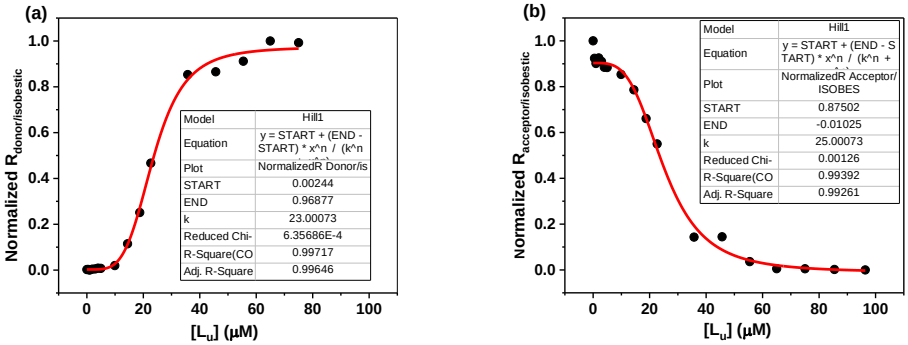

Figure S34. Normalized (a) $R_{donor/isosbestic}$ plot with concentration of unbound guest, (b) Normalized $R_{acceptor/isosbestic}$ plot with concentration of unbound guest using Merkx model for determination of association constant of RB antenna **6** with Fe^{3+}.

Table S7. Calculation of association constants (K_a) for RB **6** and RGB antenna **1** after addition of Co^{2+} and Fe^{3+}.

FRET sensor + guest system	Fitting Method + Model	K_d (μM)	R^2	Average K_d	K_a (M^{-1})
6 + Co^{2+}	**Merkx model**				
	$R_{Donor/Isosbestic}$ vs $[L_u]$	9.50	0.98	7.75 ×	12.90 ×
	$R_{Acceptor/Isosbestic}$ vs	6.00	0.98	10^{-6}	10^4
	$[L_u$				
6 + Fe^{3+}	**Merkx model**				
	$R_{Donor/Isosbestic}$ vs $[L_u]$	23.00	1.00	24.00 ×	4.17 × 10^4
	$R_{Acceptor/Isosbestic}$ vs	25.00	0.99	10^{-6}	
	$[L_u]$				
1 + Co^{2+}	**Merkx model**				
	$R_{Donor/Isosbestic}$ vs $[L_u]$	11.00	0.98	9.75 ×	10.25 ×
	$R_{Acceptor/Isosbestic}$ vs	8.50	0.99	10^{-6}	10^4
	$[L_u]$				
1 + Fe^{3+}	**Merkx model**				
	$R_{Donor/Isosbestic}$ vs $[L_u]$	34.00	0.99	34.00 ×	2.94× 10^4
	$R_{Acceptor/Isosbestic}$ vs	34.00	0.97	10^{-6}	
	$[L_u]$				

Plausible Mechanism for Co^{2+}/Fe^{3+} sensing

The plausible mechanism of modulation of the aza-BODIPY absorption band with Co^{2+} or Fe^{3+} addition (i.e., disappearance of the aza-BODIPY red absorption band) and therefore FRET turn-off mechanism in RGB antenna **1** or RB **6** has been discussed in our recent work on FRET cassettes.[S1] Aza-BODIPY is an electron deficient chromophore and highly susceptible to one electron reduction because aza-BODIPY radical anion is more aromatic than neutral aza-BODIPY. Thus, upon addition of Co^{2+}, the aza-BODIPY is converted into its radical anion that is characterized by depletion of the absorption band of aza-BODIPY. Addition of Fe^{3+} into aza-BODIPY also has similar effect where the Fe^{3+} salt might contain some amount of Fe^{2+} which can induce either oxidation or reduction of the aza-BODIPY to its radical cation or anion, both

characterized by depletion of its main absorption band as observed from spectroelectrochemical studies.[S1]

In order to obtain some insight into the plausible binding modes or mechanism, FTIR measurements were performed for aza-BODIPY **5**, aza-BODIPY **5** + Co^{2+} and aza-BODIPY **5** + Fe^{3+} (Figure S35) using KBr cell. From the FTIR spectra, it was observed that the stretching frequency of –C=N– bond (1603 cm^{-1}) of aza-BODIPY shifted to higher wave number upon addition of Co^{2+} (1720 cm^{-1}) and Fe^{3+} (1718 cm^{-1}) salts to aza-BODIPY solution in THF and subsequent evaporation of the solvent for FTIR measurement. Furthermore, new characteristic peaks around 624 cm^{-1} and 626 cm^{-1} were obtained for aza-BODIPY **5** + Co^{2+} and aza-BODIPY **5** + Fe^{3+} which could be attributed to the formation of Co^{2+}-N and Fe^{3+}-N bonds respectively[S16] Such shift of C=N stretching frequency to higher wavenumber and concomitant formation of new peaks in the 500-600 cm^{-1} region (corresponding to Co-N bond) upon binding of Co^{2+} to C=N is reported for Methylene blue compounds.[S16] Since both Co^{2+} and Fe^{3+} have strong affinity for nitrogen, they can bind to Nitrogen of –C=N– followed by the electron transfer processes that lead to decolourisation of the aza-BODIPY. NMR experiments were also attempted with aza-BODIPY with addition of Co^{2+} and Fe^{3+} however, Co^{2+} and Fe^{3+} being paramagnetic metal ions led to either paramagnetic deshielding in NMR signals or complete broadening of signals thereby preventing any further analysis.

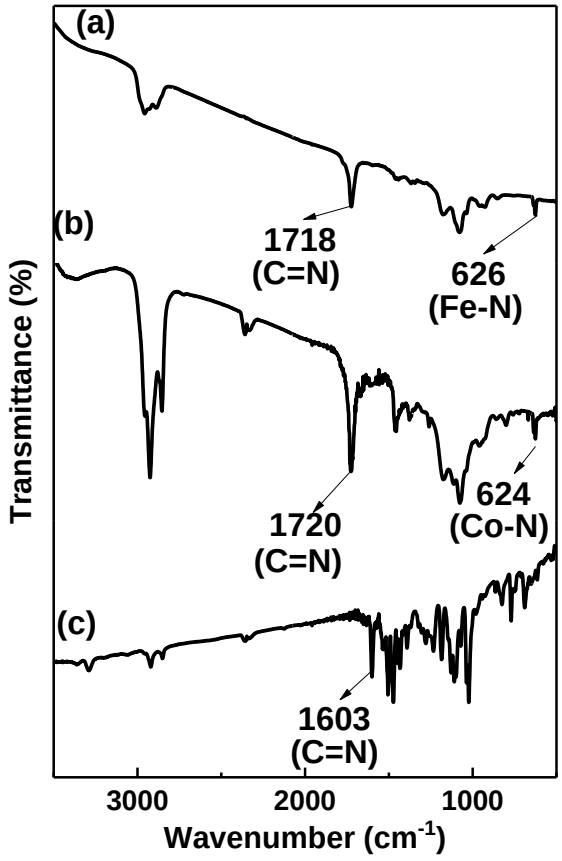

Figure S35. FTIR spectra of (a) aza-BODIPY **5** + Fe^{3+}, (b) aza-BODIPY **5** + Co^{2+} and (c) aza-BODIPY **5**.

9. Comparison table

Table S8. Comprehensive table on existing covalently/non-covalently connected RGB multichromophoric systems and their applications.

S. No.	RGB systems[a] with constituent red, green and blue chromophores	Energy transfer	Other applications	References
1.	**Dendrimers** bearing terylene tetracarboxdiimide (TDI), perylene dicarboxmonoimide (PMI) and Naphthalimide dicarboxmonoimide (NMI).	Energy transfer and energy gradient induced by different dyes located at periphery, in scaffold, and in core of polyphenylene dendrimer.	-	*Angew. Chem.* **2002**, *114*, 1980-1984.
2.	**Dendrimer** based on coumarin, fluorol and PDI	Cascade FRET without the undesired chromophore self-quenching excimer formation and ETE ~ 96 %.	-	*Chem. Commun.*, **2002**, 2605-2607
3.	**Dendrimer** based on eight napthopyranone, 16 coumarin and a central porphyrin.	Quantitative energy transfer from both donors to central Porphyrin core.	-	*Org. Lett.*, **2005**, *7*, 4451-4454.
4.	**Dendrimer** based on naphthalene monoamide (NMI), PDI and TDI	Single molecule fluorescence experiments. Highly efficient unidirectional FRET from NMI to PMIs and PMIs to TDI core by means of ensemble TCSPC.	-	*J. Am. Chem. Soc.* **2005**, *127*, 9760-9768.
5.	**Calix[4]arene-based arrays** containing up to five PDIs (two orange PDI as blue absorbers, two violet PDI as green absorbers and green PDI as red absorber)	Efficient FRET with ETE of ~ 85 %.	-	*J. Am. Chem. Soc.* **2006**, *128*, 3870-3871.
6.	**Supramolecular array with Truxene** and three different kinds of BODIPY grafted on it	Both Dexter-type (from truxene to Bodipys) and FRET (between peripheral Bodipys) contribute to the overall energy migration.	-	*J. Am. Chem. Soc.* **2009**, *131*, 6108-6110)
7.	**Hydrogen-bonded supramolecular co-polymers** based on π-conjugated oligomers containing oligo-fluorene (blue), oligo(phenylene vinylene) (green), and PDI (red).	Partial energy transfer in diluted solutions and in thin films	Solution processed OLEDs based on supramolecular polymers; white light emission.	*J. Am. Chem. Soc.* **2009**, *131*, 833-843.
8.	**Trichromophoric** sensitizer consisting of BODIPY, zinc porphyrin and squaraine	Efficient ET were observed between all chromophoric subunits that enhanced the overall conversion efficiency by 25%.	Dye sensitized solar cells (DSSC)	*Org. Lett.*, **2011**, *13*, 3944-3947.
9.	**Dendritic array** with BODIPY, monostyryl BODIPY and distyryl BODIPY.	Highly efficient energy-transfer cascades between spectrally divergent chromophores.	Dendritic solar concentrator	*Angew. Chem. Int. Ed.* **2011**, *50*, 10907-10912.

10.	**RGB Small Molecules** based on a bipolar molecular design (T-series and O-series) for solution-Processed single-layer OLEDs	-	Solution processable OLEDs	*Chem. Eur. J.* **2012**, *18*, 2707-2714.
11.	**Array** consisting of 21 chromophores including pyrene and multiple BODIPY dyes	A cascade of EET steps occurs from the rim to focal point of array	Preliminary studies indicated the array's ability to function as a sensitizer for amorphous silicon solar cells.	*J. Am. Chem. Soc.* **2013**, *135*, 11330-11344.
12.	**Supramolecular co-assembly** of organoclay and ionic chromophores, Coronene tetracarboxylate (blue fluorescence) and pure blue fluorescence and sulforhodamine G (yellow fluorescent)	Fine tuning of partial energy transfer to attain pure white light emission.	"soft-hybrids" as water-processable, high-transmittance materials for large-area-display.	*Adv. Mater.* **2013**, *25*, 1713-1718.
13.	**Fluorescent block copolymers** consisting of three different BODIPYs (absorbing in red, green and blue) in polymer backbone.	-	Luminescent pentablock co-micelles for multicolour imaging.	*Nat. Commun.* **2014**, *5*, 3372 (1-8).
14.	**Zeolite** doped with laser dyes i.e., oxazole and carbostyryl (blue), BODIPY (green-yellow), oxazine- and modified BODIPY (red)	Cascade like unidirectional FRET	Zeolite doped red, green and blue dyes as smart photoactive materials.	*Materials* **2017**, *10*, 495 (1-13).
15.	Templated **chromophore assembly on peptide scaffold** containing blue naphthalene-bisimide, red PDI and yellow ethynylpyrene (Y-Py) chromophores spatially organized through chemoselective reactions.	Energy transfer with structure-property relationship study through variation of : 1) dye properties, 2) different interchromophoric order, 3) distances, 4) orientations and 5) solvents.	-	*Chem. Eur. J.* **2018**, *24*, 16136-16148.

S.No.	**RGB systems[a] with constituent red, green and blue chromophores**	**Energy transfer**	**Sensing applications**			**Other applications**	**References**
			pH	**Temp**	**Metal ion**		
16.	RGB **Copolymer** based on poly(methyl methacrylate-co-1,8-naphthalimide derivatives-co-rhodamine derivative) (poly-(MMA-co-BNPTU-co-RhBAM)), containing naphthalimide and spirolactam Rhodamine derivative.	FRET process between BNPTU (donor) ring-opening RhBAM (acceptor) tunable by pH and Hg^{2+}.	Various emission colours by adjusting pH	-	Hg^{2+} probe Various emission colours by adjusting Hg^{2+} concentration	Full-colour emissive porous nanofibrous membranes.	*ACS Appl. Mater. Interfaces* **2017**, *9*, 16381-16396

17.	RGB **small molecule antenna** based on eight naphthalimides, two PDI and one aza-BODIPY.	Energy transfer from primary energy donor (naphthalimides) to primary acceptor (PDI) and from secondry donor (PDI) to secondry acceptor (aza-BODIPY).	Temperature sensor with positive temperature coefficient and sensitivity of 0.4 % $°C^{-1}$	pH sensor in organic solvent and semi-aqueous solvent	Co^{2+} and Fe^{3+} sensor through FRET turn-off from PDI to aza-BODIPY	Switchable or tunable fluorescent inks	Present system

[a]The class of material is indicated in bold.

10. References

S1 K. Rani, U. K. Pandey and S. Sengupta, *J. Mater. Chem. C*, 2021, **9**, 4607–4618.

S2 S. Guo, L. Ma, J. Zhao, B. Küçüköz, A. Karatay, M. Hayvali, H. G. Yaglioglu and A. Elmali, *Chem. Sci.*, 2014, **5**, 489–500.

S3 R. K. Dubey, D. Inan, S. Sengupta, E. J. R. Sudhölter, F. C. Grozema and W. F. Jager, *Chem. Sci.*, 2016, **7**, 3517–3532.

S4 G. Wagenblast, S. Ivanovici, M. A. Carvalho, 2015, European Patent 15170553.

S5 M. Fischer and J. Georges, *Chem. Phys. Lett.*, 1996, **260**, 115–118.

S6 G. Seybold and G. Wagenblast, *Dye. Pigment.*, 1989, **11**, 303–317.

S7 F. Schweighöfer, L. Dworak, C. A. Hammer, H. Gustmann, M. Zastrow, K. Rück-Braun and J. Wachtveitl, *Sci. Rep.*, 2016, **6**, 1–9.

S8 V. Sláma, V. Perlík, H. Langhals, A. Walter, T. Mančal, J. Hauer and F. Šanda, *Front. Chem.*, 2020, **8**, 1–12.

S9 I. Pugliesi, H. Langhals, H. Kauffmann and E. Riedle, *EPJ Web Conf.*, 2013, **41**, 2–4.

S10 H. Langhals, S. Poxleitner, O. Krotz, T. Pust and A. Walter, *Eur. J. Org. Chem.*, 2008, 4559–4562.

S11 H. Langhals and A. Walter, *J. Phys. Chem. A*, 2020, **124**, 1554–1560.

S12 P. R. Aswathy, S. Sharma, N. P. Tripathi and S. Sengupta, *Chem. Eur. J.*, 2019, **25**,

14870–14880.

S13 Y. Tu, Y. Yu, D. Xiao, J. Liu, Z. Zhao, Z. Liu, J. W. Y. Lam and B. Z. Tang, *Adv. Sci.*, 2020, **7**, 1–9.

S14 A. M. Hessels and M. Merkx, *ACS Sens.*, 2016, **1**, 498–502.

S15 A. Pomorski, T. Kochańczyk, A. Miłoch and A. Krężel, *Anal. Chem.*, 2013, **85**, 11479–11486.

S16 Z. Liu, X. Jia, P. Bian and Z. Ma, *Analyst*, 2014, **139**, 585–588.